



**Luís Pacheco Pereira
Neves**

**Medidas e deteção de morfologia para craniometria
usando modelos 3D**

**Measures and detection of morphology for
craniometry using 3D models**



**Luís Pacheco Pereira
Neves**

**Medidas e deteção de morfologia para craniometria
usando modelos 3D**

**Measures and detection of morphology for
craniometry using 3D models**

Dissertação apresentada à Universidade de Aveiro para cumprimento dos requisitos necessários à obtenção do grau de Mestre em Engenharia de Computadores e Telemática, realizada sob a orientação científica do Professor Doutor Paulo Miguel de Jesus Dias, Professor Auxiliar, e da Professora Doutora Maria Beatriz Alves de Sousa Santos, Professora Associada com Agregação do Departamento de Electrónica, Telecomunicações e Informática da Universidade de Aveiro.

o júri / the jury

presidente / president

Prof. Doutor Joaquim João Estrela Ribeiro Silvestre Madeira
Professor Auxiliar da Universidade de Aveiro

vogais / examiners committee

Prof. Doutora Maria Beatriz Duarte Pereira do Carmo
Professora Auxiliar da Faculdade de Ciências da Universidade de Lisboa

Prof. Doutor Paulo Miguel de Jesus Dias
Professor Auxiliar do departamento de Eletrónica, Telecomunicações e Informática da Universidade de Aveiro

**agradecimentos /
acknowledgements**

First and foremost I would like to extend my thanks and gratitude to my supervisors, Paulo Miguel de Jesus Dias and Maria Beatriz de Sousa Santos, for their advice and guidance throughout this dissertation.

I have to thank Daniel Santos, the author of the dissertation which I continued, for his availability and for helping me in the beginning when I was having trouble setting everything up.

My sincere thanks to the anthropologists, Catarina Coelho and Maria Teresa Ferreira, for all their collaboration, availability and feedback.

I would also like to thank Samuel Silva for his advice and suggestions which helped develop this dissertation.

Finally to my family and friends, for all their interest and support.

palavras-chave

Craniometria, Modelos 3D, Aquisição 3D, Estruturas 3D, Detecção de Características, Morfologia

resumo

Esta dissertação tem como objetivos principais melhorar a aplicação CraMs, Craniometric Measurements, e explorar novos métodos de medição e deteção de características morfológicas para análise craniométrica usando modelos 3D. A aplicação CraMs foi desenvolvida no ano letivo 2012-2013 no âmbito de uma dissertação de Mestrado com o objetivo de auxiliar os antropólogos no processo de realizar medições craniométricas. Através da utilização de modelos 3D e da marcação de pontos de interesse, pelos antropólogos, as medições craniométricas podem ser feitas numa aplicação de software. Este método ajuda a preservação dos espécimes e poderá reduzir a variabilidade entre medidas obtidas por diferentes especialistas. O trabalho desenvolvido nesta dissertação inclui a resolução de problemas encontrados pelos especialistas na aplicação CraMs, a deteção de mais medidas, a melhoria da experiência de utilização, bem como a exploração de novos métodos. Estes novos métodos focam-se na análise da morfologia dos espécimes e na deteção de características morfológicas, nomeadamente a forma das órbitas e a complexidade das suturas.

keywords

Craniometry, 3D Models, 3D Acquisition, 3D Structures, Feature Detection, Morphology

abstract

This dissertation focuses on improving the application CraMs, Craniometric Measurements, and exploring new methods of measuring and detecting morphological characteristics for craniometric analysis using 3D models. CraMs was developed in the academic year of 2012-2013 in the scope of a Master dissertation with the objective of aiding anthropologists in the process of performing craniometric measurements. Using 3D models and marking points of interest, the anthropologists; are able to obtain craniometric measures in a software application. Using this method helps with the preservation of the specimens and might reduce the variability in measures obtained by different specialists. The work developed in this dissertation includes solving issues found by the domain experts in the application, extending its functionalities to comprise more measures and improve user experience, as well as exploring new methods. These methods focus on morphology analysis of the specimens and on the detection of morphological characteristics, namely the shape of orbits and the complexity of sutures.

Table of Contents

Table of Contents.....	i
Index of Figures	iii
Index of Tables.....	v
1 Introduction	1
1.1 Motivation and Objectives	1
1.2 Dissertation Structure.....	2
2 Craniometry.....	3
2.1 Traditional Craniometry.....	3
2.2 Geometric Morphometrics	4
2.3 Data Set	5
2.4 3D Scanning and Skulls Acquisition	5
2.5 Points, Measures and Structures of Interest	7
3 CraMs - Craniometric Measurements.....	9
3.1 Previous version of the application	9
3.1.1 Architecture and Specifications.....	9
3.1.2 Alignment	11
3.1.3 Point selection methods	12
3.1.4 Limitations	13
3.2 Modifications and improvements to CraMs.....	14
3.2.1 Software issues	14
3.2.2 Usability issues.....	15
3.2.3 Additional features implemented	16
3.2.4 Measures using Planes	17
3.2.5 Decimation	18
4 Detection of morphological structures	21
4.1 Related work	21
4.2 Concepts used for detecting structures.....	23
4.2.1 Curvature.....	23
4.2.2 Sharp Edges	25
4.3 Orbit detection.....	26
4.3.1 Detection using curvature values.....	27

4.3.2	Detection using Sharp Edges.....	27
4.4	Suture detection.....	30
4.4.1	Detection using curvature values.....	30
4.4.2	Detection using Sharp Edges.....	31
5	Results.....	33
5.1	Overview.....	33
5.2	Craniometric Results and Discussion.....	33
5.2.1	Inter-Observer variability and error analysis.....	35
5.3	Decimation Results and Discussion.....	37
5.4	Orbit detection Results and Discussion.....	38
5.5	Suture detection Results and Discussion.....	41
6	Conclusion and Future Work.....	43
6.1	Conclusion.....	43
6.2	Future Work.....	44
	References.....	45
	Appendix A – Points of Interest.....	49
	Appendix B – Measures.....	55
	Appendix C – Tables of Measures for all (8) Skulls.....	59
	Appendix D – Tables of Measures for all (8) Skulls using Decimated models.....	63
	Appendix E – Tables of Measures for all (8) Skulls using the orbit detection method.....	65
	Appendix F – CraMs User Manual.....	67
	Appendix G – CraMs Installation and Configuration.....	76

Index of Figures

Figure 1 - Example of facial shape analysis. Image taken from (Vioarsdóttir et al., 2002).....	4
Figure 2 - Breuckmann 3D Scanner. Image taken from (Santos, 2013).....	6
Figure 3 - Work flow of the application. Adapted from (Santos, 2013).....	10
Figure 4 - Application architecture. Adapted from (Santos, 2013).....	11
Figure 5 - Craniometric planes. Adapted from (Santos, 2013).....	12
Figure 6 - Results obtained with (left) and without (right) aligned centroids in the pre-alignment phase.....	16
Figure 7 - Example of the text labels identifying marked points.....	17
Figure 8 - Parallelism between marked and reference planes, The Yellow plane is parallel to the Red plane (left) and the Cyan plane is parallel to the Blue plane (right).....	18
Figure 9 - Position of the planes and points used for the measures MAL (left) and MDH (right).....	18
Figure 10 - Edge contraction. Image taken from (Garland & Heckbert, 1997).....	20
Figure 11 - Example of decimated models. At the far left is the original model number 25, then three decimated models with 5%, 2.5% and 1% of the total number of points of the original model.	20
Figure 12 - Surface types. Concave (left), Flat (middle) and Convex (right). Image taken from (Santos, 2013).....	24
Figure 13 - Gaussian (left) and Mean (right) curvature values.....	24
Figure 14 - Orbit curvature values. Using Gaussian (left) and Mean (right) curvature using the same colour scale.....	24
Figure 15 - Sutures curvature values. Using Gaussian (left) and Mean (right) curvature using the same colour scale.....	25
Figure 16 - Sharp edges (in red) detected in sutures using Mean (top) and Gaussian (bottom) curvature values with factors (λ) 14, 25, 35, and 55, from left to right respectively.....	26
Figure 17 - Sharp edges (in red) detected in an orbit using Mean (top) and Gaussian (bottom) curvature values with factors (λ) 14, 25, 35, and 55, from left to right respectively.....	26
Figure 18 - Example of structure detected between 3 points in an orbit, in low and high resolution models respectively. The colour pattern of the spheres indicates the order in which it was found (darker to lighter).....	27
Figure 19 - Structure detected using sharp edges. The four reference points are coloured as green. The colour pattern of the spheres indicates the order in which it was found (darker to lighter).....	28

Figure 20 - Plane fitted to the structure. Frontal view (left) and side view (right).....	28
Figure 21 - Structure points projected onto the plane. The projections are represented by blue spheres. Frontal view (left) and side view (right)	29
Figure 22 - Ellipse fitted to projected points. Ellipse points are represented as red spheres, the two axis as yellow and light blue. Normal view (left) and view with hidden model (right).....	29
Figure 23 - Structure detected using 3 (left) and 7 (right) reference points. The colour pattern of the spheres indicates the order in which each section was found (darker to lighter).....	30
Figure 24 - Example of structure detected between two points in a suture, in low (left) and high (right) resolution models. The colour pattern of the spheres indicates the order in which it was found (darker to lighter).....	31
Figure 25 - Example of suture detection on the Sagittal suture. Before (top) and after (bottom) the method is applied. The main structure is represented as blue spheres and the colour pattern indicates the order in which it was found (darker to lighter). Teal spheres represent the points considered to be part of the suture.....	32
Figure 26 - Bar plot with the difference percentage for each measure between specialists using CraMs (top) and traditional methods (bottom). Automatic (green), Semi-Automatic (blue) and Manual (orange)	35
Figure 27 - Graphic with the difference percentage in relation with the original model. Model #25 (top) and Model #65 (bottom).....	38
Figure 28 - Bar plot with the difference percentage for two measures between specialists using CraMs (top) and traditional methods (bottom). OBB (number 17) and OBH (number 18).....	40
Figure 29 - Example of Sagittal suture on three skulls (65, 21 and 25) with different complexity classifications. The classifications given to these by the author are: Simple (top), Intermediate (middle) and Complex (bottom),.....	41

Index of Tables

Table 1 - List of points and the information used to define each one. "N.L." stands for Neighbourhood Level which quantifies the topological space being considered. Adapted from (Santos, 2013)	10
Table 2 - Measures calculated. Adapted from (Santos, 2013).....	10
Table 3 - Relevant points missing in the previous application (see Appendix A for more details)	14
Table 4 - Relevant measures missing in the previous application (see Appendix B for more details)	14
Table 5 - Number of vertices and faces of each original model	19
Table 6 - Number of vertices and faces of model number 25 with the different reduction percentages.....	20
Table 7 - Measure values for two specimens obtained by two Anthropologists using Crams (App) and traditional methods (Antr). Automatic (green), Semi-Automatic (blue) and Manual (orange)....	34
Table 8 - Average difference percentages obtained for each type of measure. Automatic (green), Semi-Automatic (blue) and Manual (orange)	36
Table 9 - TEM values obtained for each type of measure. Automatic (green), Semi-Automatic (blue) and Manual (orange)	37
Table 10 - Automatic measures taken on model #25 with different degrees of decimation. The percentage indicates the number of vertices in the model compared to the original	37
Table 11 - Automatic measures taken on model #65 with different degrees of decimation. The percentage indicates the number of vertices in the model compared to the original	37
Table 12 - Measures obtained by two Anthropologists using the orbit detection method (App) and traditional methods (Antr).....	39
Table 13 - TEM values obtained for the two measures OBH and OBB.....	39
Table 14 - Measures obtained from the orbit detection method.....	40
Table 15 - Results from the suture detection method for all eight specimens. The ratio is the percentage of suture points compared to the total points in the model.....	42

1 Introduction

1.1 Motivation and Objectives

This dissertation is the continuation of a previous Master dissertation done in the academic year of 2012-2013 (Santos, 2013) addressing craniometry and how the measurement process could be improved through the usage of an interactive computer system, developing an application for this purpose. The goal of the work presented is to further develop the project by improving the application developed (CraMs - Craniometric Measurements) and exploring new features related to geometric morphometrics.

Upon reading through the previous dissertation and receiving feedback directly from the anthropologists it was clear that CraMs' user interface needed to be significantly improved to be used in a real scenario. Several features also needed to be improved/expanded in order to obtain more results and further validate the approach.

Another topic of interest for anthropologists is the detection and classification of structures of interest (such as the orbits, the jaw, sutures, etc.); this led to the development of the sharp edge structure detection method for the orbits, which provided two additional measures. Preliminary work on suture detection has also been performed, as well as preliminary validation of the approach.

This project was particularly motivating given its potential to help improve the work in the field of craniometry. By integrating more technology into this field and exploring new paths, its boundaries can be pushed and grant access to new information.

1.2 Dissertation Structure

This dissertation is structured in six chapters. This chapter contains a brief introduction to the work developed.

In the second chapter (chapter 2) a brief description about traditional craniometry, geometric morphometrics and the data set are presented. Information about 3D scanning and how the acquisition process is done, and the points, measures and structures of interest used when analysing a skull are briefly described.

The third chapter (chapter 3) is devoted to the CraMs application, how it was developed, the solved issues and new features that were implemented.

Throughout the fourth chapter (chapter 4) the concepts and methods used for structure detection are explained.

The fifth chapter (chapter 5) is focused on showing all the results obtained and their discussion.

Finally the last chapter (chapter 6) presents the conclusion and future work.

2 Craniometry

This chapter encompasses the basic concepts and explanations on the field of craniometry and geometric morphometrics. The data set is presented, as well as an overall description of the 3D scanning and acquisition process. Finally a brief description of the points, measures and structures of interest used in craniometry is given.

2.1 Traditional Craniometry

The usage of craniometric measurements in the Anthropology field as a tool to identify sex, ancestry and variations in populations is well known (Buck & Vidarsdottir, 2004; Howells W., 1973; Stephens, 2000). Citing Stephens (Stephens, 2000): "The roots of anthropometry are traced back to the initial measurement of the skull by early scientists. In a simple definition, craniometry refers to the study of human cranial measurements for use in anthropological classification and comparison".

Traditional craniometry involves the physical manipulation of the skull while using specific tools to take measurements that rely on a set of landmark points (Stephens, 2000). However, the exact location of these points is different for each skull due to differences in shape, which means that different Anthropologists, or even the same Anthropologist on different occasions, might perceive them in slightly different locations when taking the measurements. Although the levels of intra- and inter- observer errors tend to be reasonable, in some cases they might be significant enough to invalidate the usage of certain measurements.

2.2 Geometric Morphometrics

The analysis and quantitative representation of morphological shapes is called Geometric Morphometrics. Through the study of the geometry of a morphological structure, several landmarks can be determined. These landmarks might not be solely defined by points, similar to the traditional craniometric points, they might be defined by lines or other known shapes as well. By comparing the characteristics of these landmarks on similar structures they can be categorized and new information can be gathered for further usage in studies (Buck & Vidarsdottir, 2004; Gonzalez, Bernal, & Perez, 2011; S. Sholts, Walker, Miller, & Wärmländer, 2007; Vioarsdóttir, O'Higgins, & Stringer, 2002). Applied to skulls these methods can be used to classify, for example, the cranial shape in a given population (Baylac & Friess, 2005). Figure 1 shows an example of facial shape analysis using transformation grids. This was used to study different populations and their distinctive facial features and proportions.

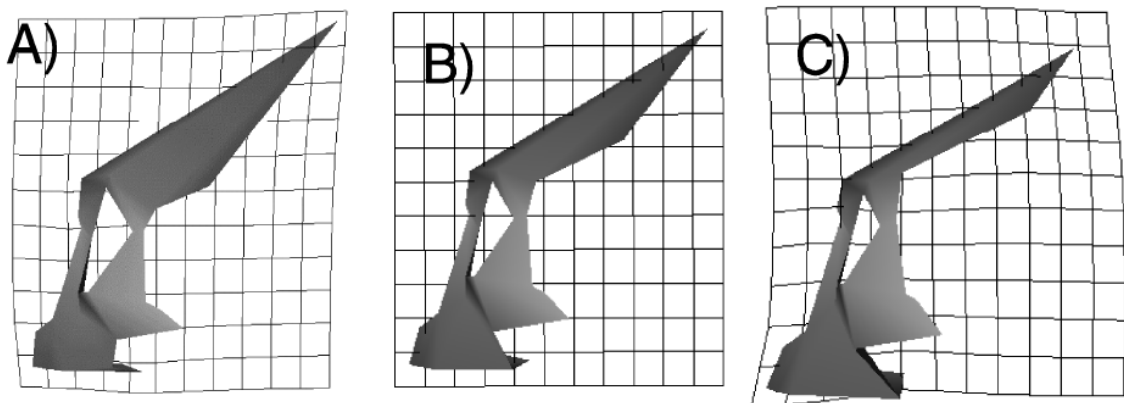


Figure 1 - Example of facial shape analysis. Image taken from (Vioarsdóttir et al., 2002)

These methods have been criticized for being prone to subjectivity (Gonzalez et al., 2011; Hefner, 2009; Ross, Ph, Slice, & Williams, 2010; S. B. Sholts, Walker, Kuzminsky, Miller, & Wärmländer, 2011; S. Sholts et al., 2007). Citing Hefner (Hefner, 2009): "The experience based method of ancestry prediction using morphoscopic traits indeed is an art: an art that is intuitive, untestable, unempirical, and consequently unscientific. It is often more appropriate to perform a metric analysis when working with morphological data, since it has proven to be more objective". However, through the usage of technology and with the development of advanced algorithms these methods might become more objective and have an increased repeatability (Weber, 2013). Weber explains in great detail how the Geometric Morphometrics approach can be used and the advantages it can have when used to extract and analyse information from 3D models.

2.3 Data Set

Since this dissertation is the continuation of (Santos, 2013) the data set remains the same. In 2009 a rescue excavation was performed at the *Vale da Gafaria* by a team from iDryas, the site is located outside the modern and medieval walls of the city of Lagos in Portugal (Neves, Almeida, & Ferreira, 2010, 2011). This site, active between the 15th and 17th centuries, revealed two occupations. Eleven individuals were recovered from one of them which was a part of Lagos Leprosarium, only known from historical documents (Neves et al., 2010, 2011). However, from the other occupation, which was an urban discard deposit with an area of more than 1000m² and a stratigraphic thickness of several meters, the remains of 155 individuals were exhumed.

The collection of skulls is composed of 64 cranial and mandibular remains from 60 slaves and 4 leprosy sufferers, which all had an age of death above 18 years old, including 30 females, 20 males and 14 undetermined. In terms of preservation: 38% have the complete skulls and mandibles, 14% were reconstructed manually by the anthropologists team and 48% were fragmented.

There is a worldwide lack of osteoarchaeological series that can illustrate the earliest phase of the European Atlantic expansion (Hefner, 2009), due to this fact the results obtained in the preliminary research done with the Lagos collection are a pioneering attempt to characterize African slaves. In relation with the history of the modern Atlantic commerce of African slaves, most of the excavated necropolises date from later periods, between the 17th and 19th centuries and were found in the New World (Blakey, 2001). Moreover, all the anthropological analyses of African slaves' populations relied solely on direct observation of the osteological specimens and most were not conducted extensively (Hefner, 2009). This suggests that the Lagos collection has the potential to provide relevant archaeological and anthropological results.

2.4 3D Scanning and Skulls Acquisition

Not so long ago all studies and analyses in the fields of archaeology and biological anthropology had to be made manually and on the physical specimens. This meant that the specimens could be easily damaged or get lost while travelling. Considering these problems and the evolution of digital technologies in the recent decades, the advantages of an integration of these technologies into these fields became clear, as stated in several articles (Balzeau et al., 2010; Wachowiak & Karas, 2009; Weber, 2013). Citing Weber (Weber, 2013): "Virtual Anthropology (VA) exploits digital technologies and brings together experts from different domains such as anthropology, biology, medi-

cine, mathematics, statistics, computer science, and engineering. VA mainly deals with the functional morphology of recent and fossil hominoids. Its methods can, of course, be applied in a much broader sense".

There are many 3D scanning techniques capable of producing high precision tridimensional digital models although not all of them exclude physical manipulation of the object being scanned. Since preservation is especially important when dealing with human osteoarchaeological remains the most adequate scanning techniques are those that do not involve any kind of physical contact. The specimens referred throughout this dissertation were scanned using a Breuckmann SmartSCAN¹ structured light scanner shown in Figure 2. This scanner projects a set of stripe patterns onto the object and extracts its geometry by comparing the known projected patterns with the projected image of the pattern. This process is repeated several times while rotating the object and adjusting the pattern and light setup in order to obtain a complete and precise 3D model. The acquisition was done by a team from iDryas, including a 3D acquisition technician and several anthropologists to ensure the process would capture all the important sections of the skulls. Further details about the scanning and acquisition process can be found in (Santos, 2013).



Figure 2 - Breuckmann 3D Scanner. Image taken from (Santos, 2013)

¹ <http://aicon3d.com/products/breuckmann-scanner/smartscan>

2.5 Points, Measures and Structures of Interest

As explained earlier, in craniometry a set of landmark points are defined throughout the whole skull. Several of these points are essential to perform the 24 measures the anthropologists at iDryas use (see Appendix B for more details). Initially 21 points were defined as being of interest (see appendix A for more details); however, some additional points were used in order to accomplish specific measures, for example the measurements that use projections (MAL and MDH).

Since the measurements are performed repeatedly by one or more specialists, two types of errors must be considered:

1. Inter-observer error: the difference between the interpretations of two or more individuals observing the same phenomenon;
2. Intra-observer error: the difference between the interpretations of an individual observing the same phenomenon at different times.

Technology keeps evolving, becoming more precise and complex. Through its integration in this field, it might be possible to reduce variability between observers and increase repeatability in measurements.

In terms of structures of interest, skulls have a large amount of characteristics that can be used to perform studies. Considering these characteristics as structures of interest means they can be used for shape or volume comparisons. These structures are defined by the shape of the bone in the specific area of the skull. Information about volume, shape differences, distances, etc. can be extracted from them. Some examples that are commonly seen in studies are facial proportions and changes in the overall skull appearance (angle and size differences).

3 CraMs - Craniometric Measurements

In this chapter is presented a portrait of the application known as CraMs. The chapter is divided into two sections, the first one illustrating the previous state of the application and the second one explaining the main improvements to the application performed within this work.

3.1 Previous version of the application

This section briefly describes the status of the application developed in (Santos, 2013), which was the starting point of this work. It presents its architecture and specifications, a brief description of how the alignment process works, the point selection methods that were used and the limitations found by the domain experts that used it.

3.1.1 Architecture and Specifications

The application developed in (Santos, 2013) followed the work flow shown in Figure 3. The skull models acquisition process is briefly explained in section 2.4. After a model is loaded it is necessary to align it properly, through manual alignment or through ICP (Iterative Closest Points) using a template model (which is already aligned). After the alignment phase some points can be detected automatically by the application. The detection of additional points is fully manual or uses curvature/alignment information to find the best matching point. Table 1 shows the list of points that can be marked and based on what information they are defined, the acronym "N.L." stands for Neighbourhood Level and quantifies the topological space that is taken into consideration. Finally, based on the marked points, the possible measures are calculated, shown in Table 2.

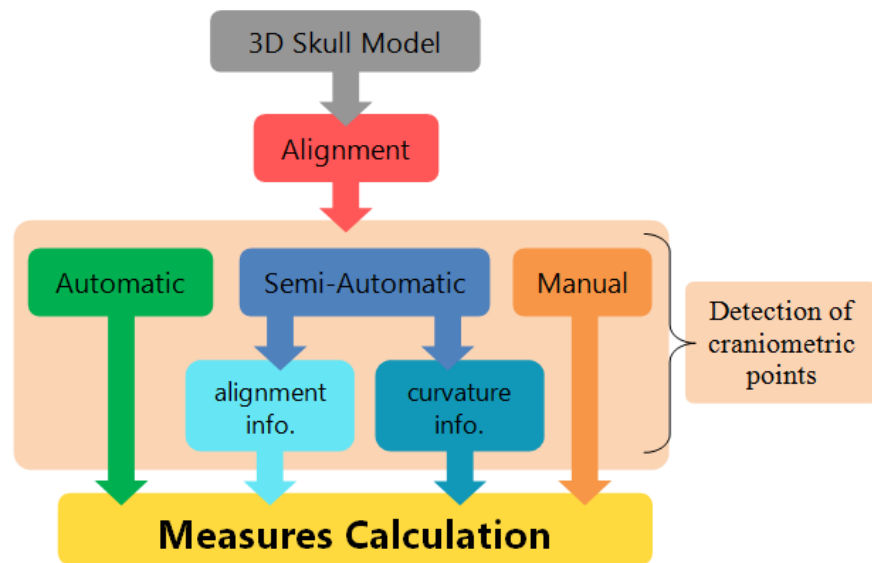


Figure 3 - Work flow of the application. Adapted from (Santos, 2013)

Point	Information used (details)
Zygion (bilateral)	Coordinates (max & min X with negative Y)
Basion	Coordinates (min Y on Z axis)
Vertex	Coordinates (max Y)
Bregma	Coordinates (min Y in coronal suture)
Opisthokranion	Coordinates (min Z on Frankfurt plane)
Lateral Sagittal Plane (bilateral)	Coordinates (max & min X with $Z \leq 0$)
Glabella	Curvature (<i>convex</i> with 5 N.L.)
Nasion	Curvature (<i>concave</i> with 10 N.L.)
Prosthion	Curvature (<i>concave</i> with 5 N.L.)
Ektomalare (bilateral)	Curvature (<i>convex</i> with 3 N.L.)
Biauricular (bilateral)	Curvature (<i>concave</i> with 3 N.L.)
Nasospinale	Curvature (<i>concave</i> with 10 N.L.)
Frontomolare-Temporale (bilateral)	Curvature (<i>convex</i> with 3 N.L.)

Table 1 - List of points and the information used to define each one (see Appendix A for more details). "N.L." stands for Neighbourhood Level which quantifies the topological space being considered. Adapted from (Santos, 2013)

ZYB	BBH	BPL	AUB
XCB	BNL	UFHT	NLH
GOL	FRC	MAB	UFBR

Table 2 - Measures calculated (see Appendix B for more details). Adapted from (Santos, 2013)

The application was developed using the C++ Programming Language. VTK was used for the 3D visualization and interaction parts, and Qt was used to build the user interface. VTK and Qt run on

top of the operating system, as shown in Figure 4, while exchanging messages in order to make possible the API's integration (visualization, interaction, windowing system, etc.). The application has four distinct modules:

Tools: developed methods to analyse models, take care of alignment, find points of interest, etc.

GUI: graphical user interface containing all the Qt code that handles window creation, menus, etc.

Interaction: contains all code necessary to handle the interaction with the models.

Utils: contains some utility functions and structures.

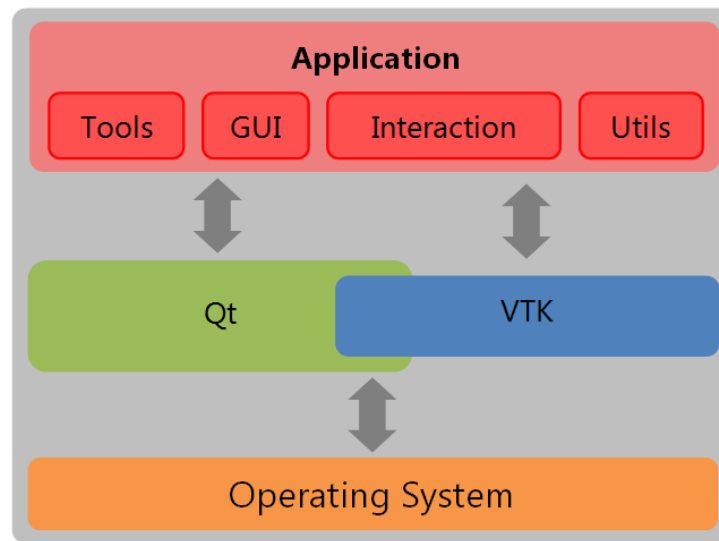


Figure 4 - Application architecture. Adapted from (Santos, 2013)

3.1.2 Alignment

During the acquisition process of the 3D models or when performing measurements using traditional methods, the alignment of the skulls is not taken into account since they are positioned and manipulated to obtain the best results. However, being able to have the model aligned when working with it virtually is very important. By having it aligned three reference planes (Coronal, Sagittal and Frankfurt) can be properly defined (as shown in Figure 5). These provide additional information to the application, which improves the detection of landmark points. The model can be divided into several sections, left and right, front and back, and top and bottom by visualizing the reference planes.

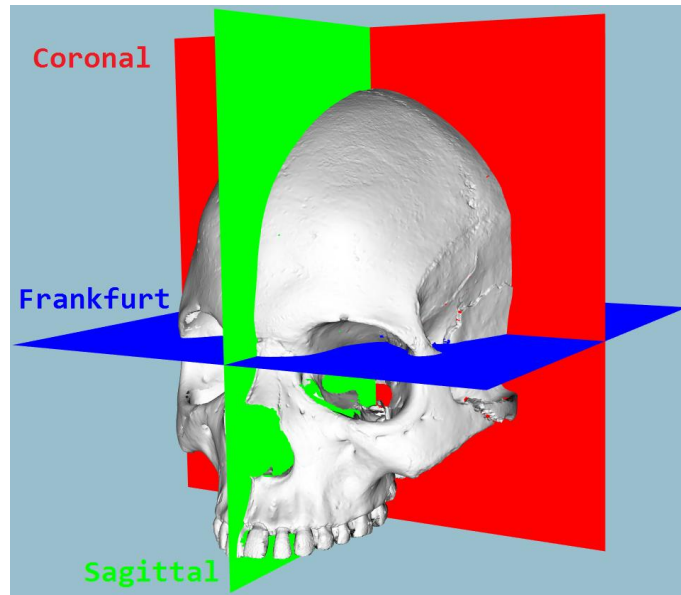


Figure 5 - Craniometric planes. Adapted from (Santos, 2013)

In this version of the application the alignment could be done using two methods:

- Manually: The user locates seven landmark points on the loaded model and based on their position the skull is aligned;
- Semi-Automatically: Through the usage of a template (already aligned), the user can visually compare and rotate the model to adjust its orientation and provide a better first estimate, then the ICP algorithm (Besl & McKay, 1992) overlaps the two (model and template) and tries to minimize the difference between them.

Although the alignment methods still have some robustness issues, as a starting point they are easy to use and serve their purpose.

3.1.3 Point selection methods

In order to perform craniometric measurements, landmark points are needed as explained earlier. There are three methods to select these points:

1. Manually: The user picks the position of the point without any additional help from the application;
2. Automatically: The application finds several points based on the reference planes and the location of specific regions on the aligned skull, for example, the point on the top of the skull that belongs to both sagittal and coronal planes;

3. Semi-Automatically: The user provides an initial guess of where the point should be and then based on its neighbourhood, its curvature or its coordinates (or combinations of these) the application finds the point that has the most similar characteristics to the target landmark point.

The information (neighbourhood, curvature and coordinates) that the application uses to find each point can be adjusted to obtain better results. The neighbourhood level can be adjusted to any natural number higher than two (which is the minimum), however this increases complexity and might reduce the performance of the application. The type of curvature can be set to convex or concave in order to better match the point being located. The coordinates can be used to find, for example, the point contained in the model which has the highest coordinate(s) in relation to one or more of the reference axis.

3.1.4 Limitations

After using the application to obtain all the measures presented by (Santos, 2013) the Anthropologists found several limitations. Some of them were just small details; others heavily influenced the user interaction. The main issues found were:

Software issues:

- The application stops responding in some unexpected situations;
- Some of the skull models cannot be properly aligned using the semi-automatic alignment method (influencing the points that are marked automatically). Since the rotations done in the pre-alignment phase are not being taken into consideration the alignment algorithm is not able to find a good result if the original orientation of the two models is not similar.

Usability issues:

- List of points that need to be marked for the Manual Alignment disappears and cannot be brought back into focus;
- It is not possible to delete points that were marked;
- It is not possible to correct the points that were marked automatically;
- The user has no feedback to identify which points have been marked;
- The size of the displayed spheres that represent marked points is too big;

- Lack of consistency in interaction (when marking points manually a key needs to be pressed before each mouse click but when marking semi-automatic points no key needs to be pressed before each mouse click).

Points and Measures not integrated in the application:

- There are 11 of the reference points the domain experts use for measurements missing:

Lambda	Alveolon
Right Zygomaxillare	Left Zygomaxillare
Right Frontotemporale	Left Frontotemporale
Right Dakyon	Left Dakyon
Right Ektokonchion	Left Ektokonchion
Opisthion	

Table 3 - Relevant points missing in the previous application (see Appendix A for more details)

- There are 12 measures used by the domain experts which cannot be obtained:

WFB	NLB	OBB	EKB
DKB	PAC	OCC	FOL
FOB	MAL	OBH	MDH

Table 4 - Relevant measures missing in the previous application (see Appendix B for more details)

3.2 Modifications and improvements to CraMs

After reading through (Santos, 2013) and having meetings with the field specialists, in which they gave a lot of feedback and pointed out some issues with the application, the first stage of this work was to address some problems and incorporate new features to attend to the specialists' needs. In this section these improvements and new features are presented.

3.2.1 Software issues

In some situations the application was not ready to handle the user interaction, for example when the user tried to compute measures without any marked points. Several verifications were added in order to prevent these situations from happening. Feedback for the user was added with a couple of warning pop-ups, containing information of what was missing and on which feature.

When the skull model under study is on the pre-alignment phase (as shown in Figure 6) it can be manually rotated (around each respective axis) using the keyboard keys "X", "Y" and "Z" to rotate

the model. These were implemented to help provide a better initial guess for the ICP algorithm. The rotations performed on the model are now being taken into consideration on the alignment process (previously they were not).

3.2.2 Usability issues

Manual alignment:

One of the issues pointed out by the specialists that had been using the application concerned the manual alignment. The list of points required (with their names and order) would only be shown in a pop-up window that could not be opened again once closed. The specialists would have to memorize it or write it down. In order to avoid this problem the same list of points is printed in the console window when the pop-up is brought up at the beginning of the manual alignment process.

Marked points:

The size of the marked points (spheres) was reduced as requested by the specialists. The colour of each sphere was changed to represent different types of points. Automatic points are represented in pink, semi-automatic points are represented in blue, manual points are represented in yellow and extra points (which have no name in the Figures shown in Appendix A) are represented in green.

Measures output file:

In the previous version of CraMs only the list of measures (with their name and value) would be saved on to a file when the measurement process was finished. Additional information was included on this file in order to provide more details about who was performing the measurements and when, which model was being used and the coordinates of all the marked points (which can be later used to verify measures or continue the selection process). Other improvements were made to allow the user to choose the destination of the file and its name. The application automatically suggests a name with the following structure: "username_model.txt".

Measures computation:

One of the main improvements consisted of allowing the user to compute the measures based on the selected landmarks and save at any point during the measurement process. Previously the user would have to mark all points before the application could calculate the measures. Since the user may only want to do a specific measurement between two points he/she should not have to mark all of them. In the latest version, the user may calculate the possible measures for the points that are marked, a warning will pop-up containing the names of all the missing points but the user may proceed.

Correcting marked points:

Any point that is marked on the model can now be deleted and marked again by the user. This was an important issue for the specialists. Since all points are marked using the location of the mouse pointer (as an initial or final position) and taking into account that all of the models have several gaps or holes (some natural and some corresponding to fractures) it is essential that the point picking process allows the user to undo and re-pick a point.

Semi-Automatic alignment:

An option to align the models centroids when a template is loaded was added in order to aid the user in case the template model and the model under study were displayed too far apart, which could increase the difficulty of pre-aligning the two models to provide a better initial guess to the ICP algorithm. Shown in Figure 6 are the different results obtained for the same model with (left) and without (right) this option enabled.

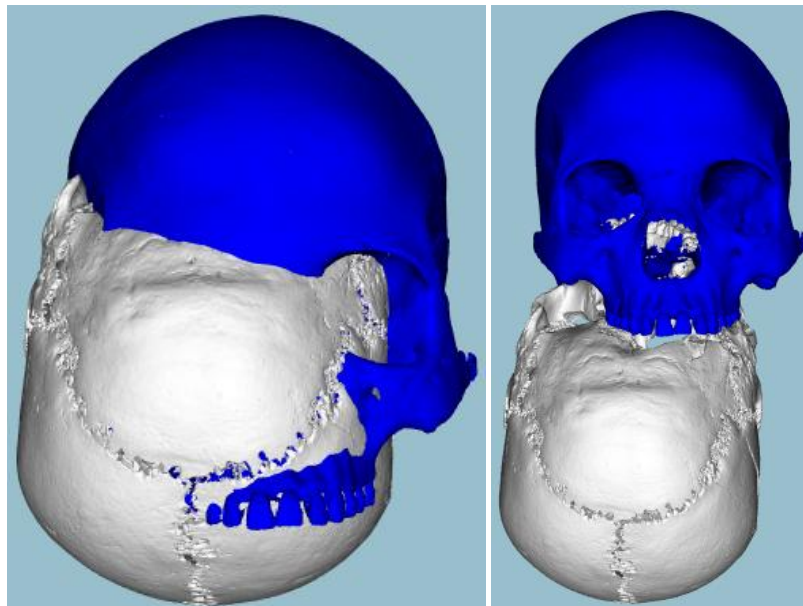


Figure 6 - Results obtained with (left) and without (right) aligned centroids in the pre-alignment phase

3.2.3 Additional features implemented

In order to solve some of the issues found by the domain experts, as mentioned earlier, new features had to be implemented.

Missing points and measures:

To tackle the issue of missing points and measures, the picking process was changed to allow the user to mark those specific points manually. Even though the process is fully manual and prone to larger errors, it allows the specialists to obtain all the measures they use. The more measures are

that taken with the application the more comprehensive the comparisons with the traditional methods can be.

Point identification:

Text labels were added to each point with its name (as shown in Figure 7). This allows the user to check the names of incorrectly marked points, which was not possible before. Labels were coloured to match the type of point they represent. They can be shown or hidden as a whole or by category.



Figure 7 - Example of the text labels identifying marked points

Measurements that use projections:

Since two of the measures from the traditional methods use projections, namely MAL and MDH (measures 23 and 24 in Appendix B), an option to define relevant planes was added. Further details are explained in the next section.

3.2.4 Measures using Planes

As explained previously, there are two measures that require the usage of a projection in a specific plane in order to obtain their value. This value is the minimum distance between a point of interest and a reference plane. These measurements are very difficult to take precisely by anthropologists with traditional methods, even when taken by the same expert repeatedly. Due to this variability these measures are not considered in most craniometric studies. In order to tackle this problem, a method was developed to allow the user to define planes of interest. In this method the user picks a point and the coordinate of interest is used to define the reference plane. The marked planes are always parallel to the respective reference planes as shown in Figure 8. Figure 9 illustrates an example of how the two measurements are taken using the planes and the points marked, each measure is the orthogonal distance from the point to the respective plane.

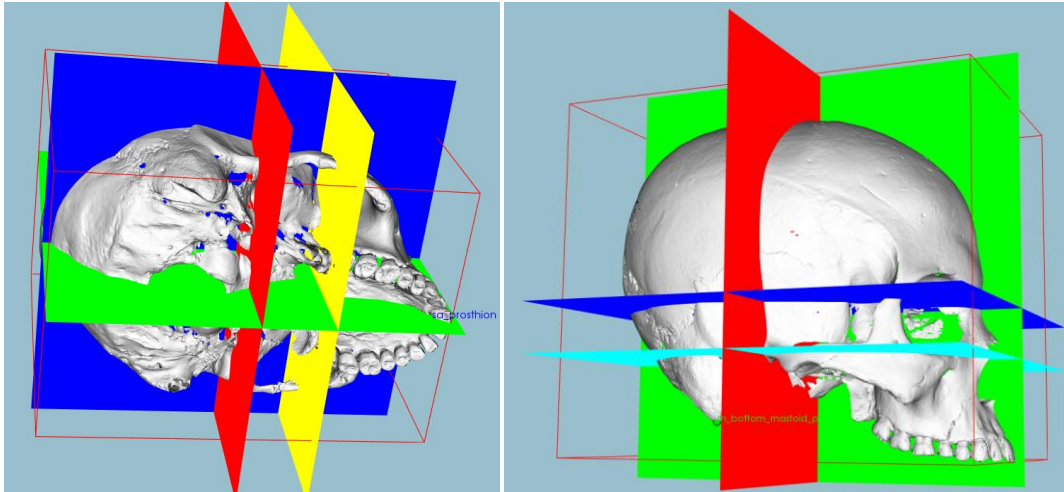


Figure 8 - Parallelism between marked and reference planes, The Yellow plane is parallel to the Red plane (left) and the Cyan plane is parallel to the Blue plane (right)

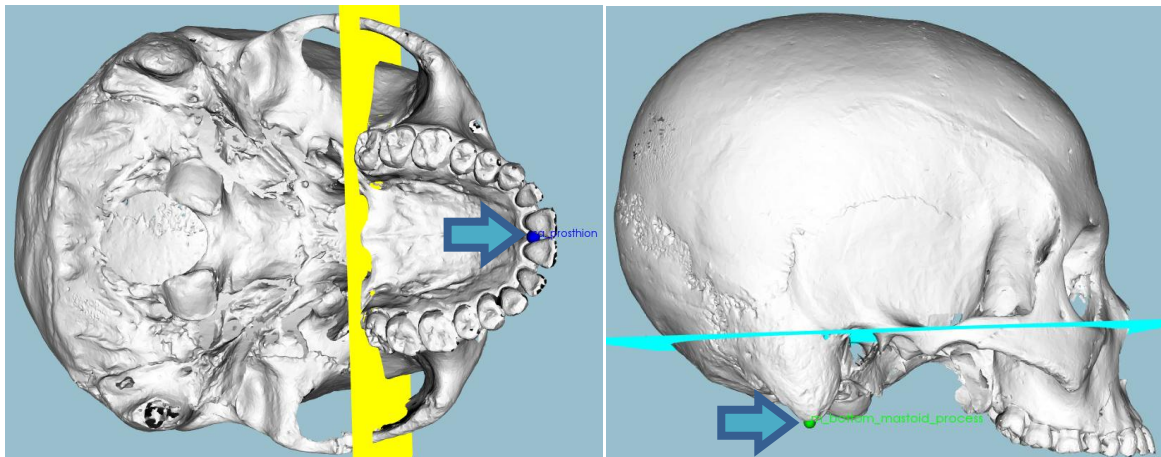


Figure 9 - Position of the planes and points used for the measures MAL (left) and MDH (right)

3.2.5 Decimation

Given the high resolution of the models, as shown in Table 5, they require a large amount of computational resources to display and process. This can have a significant impact on user interaction especially when running on a computer without any dedicated graphics hardware (as is the case of most anthropologists' PCs). Typically the users complained because the application ran slowly and each interaction took much longer than expected. In order to address this problem a preliminary study was performed to determine if the usage of models with lower resolution would have a significant influence on the precision of the measures obtained.

The main objective of decimation is to reduce the complexity of a model. Although the basic concept is to reduce the number of vertices and faces, there are several ways in which this can be

achieved (Gahm, 2010). By applying different algorithms the result can more or less maintain the original shape (faces orientation, etc.).

Model	Number of vertices	Number of faces
#21	1.370.198	2.695.036
#25	1.512.605	2.997.265
#38	1.801.451	3.566.862
#39	1.849.701	3.663.523
#57	2.096.164	4.153.290
#65	1.711.944	3.377.298
#66	2.440.999	4.843.788
#67	2.229.845	4.416.773

Table 5 - Number of vertices and faces of each original model

In order to perform this study eight skull models were decimated. Each model was decimated eight times with the same parameters but using a different reduction percentage each time (between 80 and 5%); two of the models were decimated two extra times with a 2,5 and 1% reduction percentage to obtain more extensive results (see Table 6 for an example). All decimations were done using (Meshlab, 2014) by applying the Quadric Edge Collapse Decimation filter, which tries to preserve the shape and appearance of the original model as much as possible. This filter applies an algorithm based on the *quadric error metrics* presented by Garland (Garland & Heckbert, 1997). The algorithm is built around edge-collapsing, which consists of picking a pair of vertices and contracting them to a single vertex, redefining all the triangles connected to them and discarding triangles that use both vertices, as shown in Figure 10. To get a notion of the cost of an edge contraction, a matrix \mathbf{Q} is associated with each vertex and the error is calculated, the authors call this Error Quadrics. Citing Garland: "The algorithm itself can be quickly summarized as follows:

1. Compute the \mathbf{Q} matrices for all initial vertices.
2. Select the valid pairs.
3. Compute the optimal contraction target $\bar{\mathbf{v}}$ for each valid pair $(\mathbf{v}_1, \mathbf{v}_2)$. The error $\bar{\mathbf{v}}^T(\mathbf{Q}_1 + \mathbf{Q}_2)\bar{\mathbf{v}}$ of this target vertex becomes the cost of contracting that pair.
4. Place all pairs in a heap keyed on cost with the minimum cost pair at the top.
5. Iteratively remove the pair $(\mathbf{v}_1, \mathbf{v}_2)$ of least cost from the heap, contract this pair, and update the costs of all valid pairs involving \mathbf{v}_1 ."

	Specimen #25								
	100%	80%	60%	40%	20%	10%	5%	2,5%	1%
Number of vertices	1.512.605	1.212.878	913.152	613.425	313.699	163.835	107.191	51.438	30.530
Number of faces	2.997.265	2.397.811	1.798.359	1.198.905	599.453	299.725	178.342	74.931	33.115

Table 6 - Number of vertices and faces of model number 25 with the different reduction percentages.

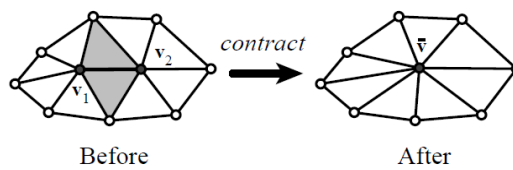


Figure 10 - Edge contraction. Image taken from (Garland & Heckbert, 1997)

By controlling which of the pairs are considered valid and the minimum error accepted, the simplification process can be tuned to produce a result that maintains the appearance of the original model as much as possible. An example of the decimation results obtained is shown in Figure 11. Even having only 2,5% the number of points of the original model, the overall appearance remains very similar to the original. This shows the level of detail and complexity of the original models and how the decimation process influences the appearance of the model.

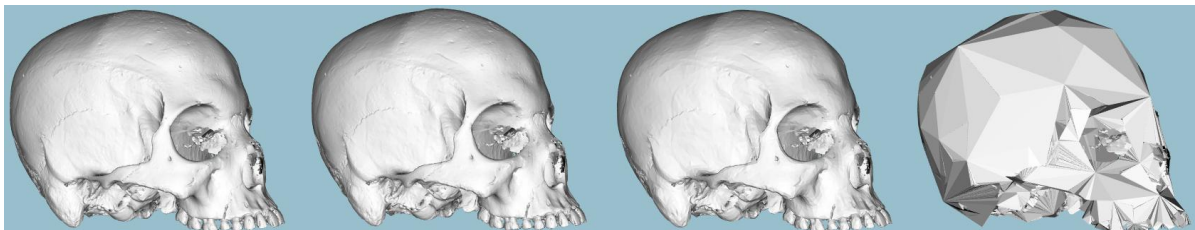


Figure 11 - Example of decimated models. At the far left is the original model number 25, then three decimated models with 5%, 2.5% and 1% of the total number of points of the original model.

Some of the decimated models were shown to the domain experts. Even though they notice some loss of detail (mostly on edges such as the teeth or the sutures) they mentioned that some degree of decimation should not significantly influence measures obtained. Due to these conclusions and the analysis of the results obtained, the acquisition process has been changed to acquire models with slightly less resolution. Further studies can be done to more precisely validate the influence of decimation in measures.

4 Detection of morphological structures

Morphological studies are still scarcely used in craniometry, mainly due to the difficulty of quantifying shapes and structures using traditional craniometry. The possibility of extracting and quantifying morphological structures consistently within a software application such as CraMs may open new doors and allow the usage of morphological information as a valid source of information in future craniometric studies. Though skulls have several structures of interest that could be used for shape or volume comparisons some choice had to be done. After meetings with the domain experts and analysing the possibilities, considering the resources and time available, the focus was on two structures of particular interest according to the anthropologists. These were the orbits (bone cavities in which the eyeballs reside), with the objective of retrieving its shape and two measures (OBB and OBH), and the sutures (fibrous joints that bind together all the skull bones), with the objective of establishing a more reliable method of classification.

4.1 Related work

Morphological shape extraction is closely related to Feature Detection or Feature Extraction. There are some interesting papers on these topics; however, only some of the articles found focus on 3D polygonal meshes (Lai, Zhou, Hu, Wallner, & Pottmann, 2007; Li & Fan, 2013; Watanabe & Belyaev, 2001). Others focus on 3D point clouds instead of polygonal meshes (An, Li, & Shao, 2013; Gumhold, Macleod, & Wang, 2001; Pauly, Keiser, & Gross, 2003), yet they present concepts relevant to this work.

In the article by Gumhold (Gumhold et al., 2001) a method to extract feature lines from a 3D point cloud is described. This method consists of five steps, first the neighborhood of each point is determined, then each point is classified as being a surface, crease, border or corner point based on which type of ellipsoid best fits it (taking into account its neighborhood). Each point has a penalty weight assigned to it which indicates the unlikelihood of it being part of a feature and based on these weight values, minimum spanning patterns are found. From these patterns the short branches are cut off to obtain single lines which are then smoothed in order to obtain the feature lines. The method proposed by Pauly (Pauly et al., 2003) is very similar to the one described by Gumhold (Gumhold et al., 2001); however, Pauly extends it by using multi-scale classification which allows for a more robust extraction of features on noisy surfaces. This multi-scale classification is based on surface variation using different neighborhood sizes which is very similar to applying a smoothing filter as the neighborhood size is increased.

Proposed by An (An et al., 2013) is a method for feature extraction from 3D point clouds based on discrete curves. In this method the discrete curves are extracted from the points and their respective neighborhoods. Using these curves several characteristics are analyzed such as angle variations, principal curvatures and the behaviors of chord lengths. Based on these characteristics, similarity indicators are defined and using these indicators the geometric features of the respective 3D point cloud data can be extracted.

In the article by Watanabe and Belyaev (Watanabe & Belyaev, 2001) an approach to detect salient curvature features is presented. This method uses a combination of mean and Gaussian curvatures as well as an "area degenerating" effect, called focal surfaces, near the model's singularities. The focal surface effect functions like a skeleton for the curvature values, for example, behind each bump in the model there is a focal rib. Through the analysis of the extreme values in curvature, ridges and ravines, and with the information provided by the focal sheet of the model, the detection of features can be achieved.

Proposed by Lai (Lai et al., 2007) is an approach to robustly classify and edit features, this approach uses integral invariants in conjunction with a remeshing algorithm to recognize features. The remeshing algorithm basically defines a new mesh of triangles surrounding the model and based on the type of triangle that is used to define specific regions, isotropic or anisotropic, it is possible to assess if the region contains a feature. This algorithm is feature sensitive but uses a weight value that should be adjusted to the model size.

The method proposed by Li and Fan (Li & Fan, 2013) mentions the integral invariants used by Lai (Lai et al., 2007) and uses them to calculate what they call 'Principal Curvature Direction' which is then used to detect relevant points in the model. The results from using four different approaches are compared. These approaches are the usage of curvature values, two fitting methods and their proposition using integral invariants.

A starting point had to be defined. After reading through the articles mentioned above the most used characteristic seemed to be the curvature values. Since the work under development is new and considering that the curvature values had already been used in CraMs, it seemed like the best path to start with. The plan was to initially detect a set of points of interest based on their curvature values and define a structure containing all of those points. Due to the simplicity of this method, results could be obtained quickly in order to validate the approach and to get an idea of how to improve it.

4.2 Concepts used for detecting structures

In this section the concepts used to detect the relevant structures are explained. Due to the complexity of the objective and since this is an initial approach a semi-automatic method was chosen. The method requires manual selection of seed points by the user. It then tries to find a structure using these reference points and the characteristics of the model surrounding them. Through the usage of these reference points some control over the results can be maintained and useful information can be extracted for further developments.

4.2.1 Curvature

As mentioned earlier curvature values tend to provide very useful information when performing analysis on 3D models. These values are obtained by extracting the information about the type and degree of curvature on a surface. In order to extract this information the *Principal Curvatures* have to be defined. These consist of the maximum and minimum of the *Normal Curvatures* at the surface point. Normal curvatures are the curvatures of the curves on the surface that intersect with the planes that include the tangent vector and the surface normal. The principal curvatures are then used to calculate the Gaussian and Mean curvature values for each point on the surface:

- Gaussian curvature: The product of the principal curvatures;
- Mean curvature: Half the sum of the principal curvatures.

By calculating the curvature values the surface can be classified as one of three types:

- Concave: Has an inward curvature, looks like a saddle;
- Flat: Has no curvature in at least one direction;
- Convex: Has an outward curvature, looks like a bowl.

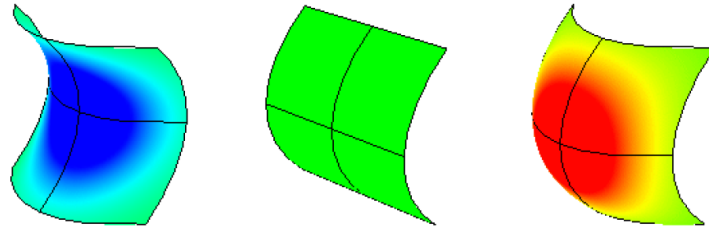


Figure 12 - Surface types. Concave (left), Flat (middle) and Convex (right). Image taken from (Santos, 2013)

The curvature values of the model were calculated using the implementation provided by VTK. Then they were represented using a colour scale as shown in Figure 13. Figure 14 and Figure 15 show the structures of interest in this work (orbit and sutures). By visually analysing the variability in curvature values near these two structures it seems that the points with a relevant curvature value could be used to aid in extracting their shape. After consulting the specialists on this matter they agreed that this could be a valid approach.

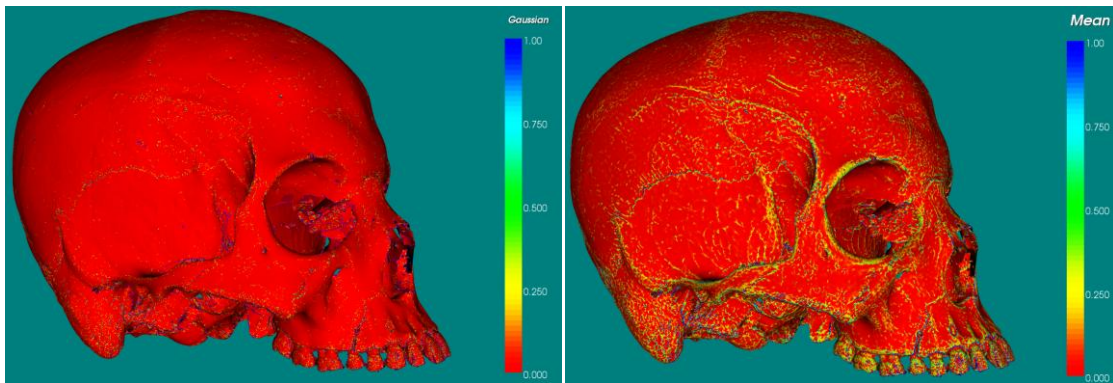


Figure 13 - Gaussian (left) and Mean (right) curvature values

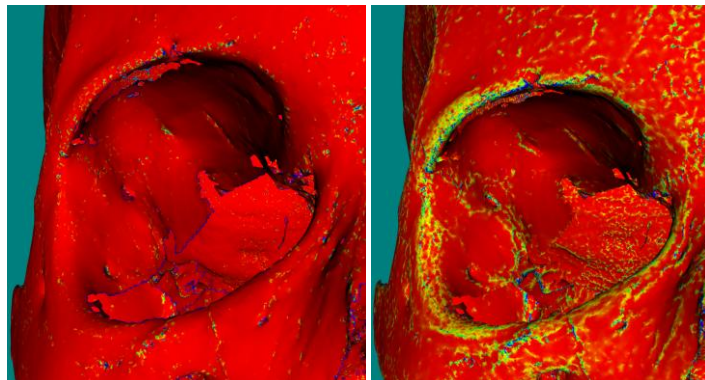


Figure 14 - Orbit curvature values. Using Gaussian (left) and Mean (right) curvature using the same colour scale

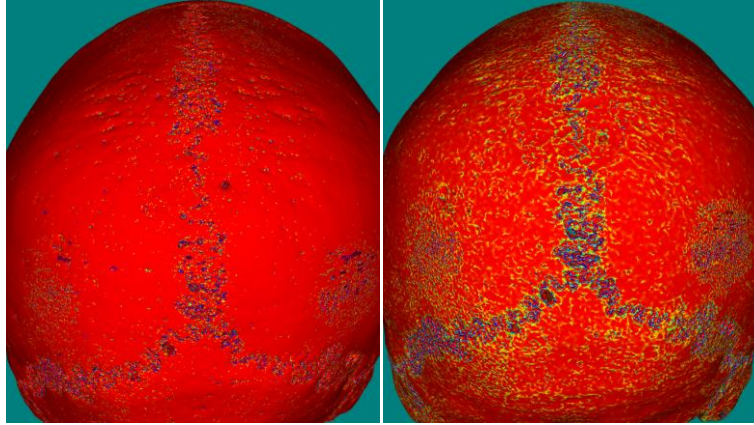


Figure 15 - Sutures curvature values. Using Gaussian (left) and Mean (right) curvature using the same colour scale

4.2.2 Sharp Edges

The initial results obtained using curvature were a good starting point. However, improvements could be made and the next step had to be defined. A possible improvement was the use of a method called *Region Growing* to perform an additional filtering of the points with high curvature. This method was described by Vieira and Shimada (Vieira & Shimada, 2005) and uses a concept which they call *Sharp Edges*. The algorithm to classify a point as a sharp edge is simple and easy to implement. However, due to the fact that the high resolution models have so many points, running the algorithm for each point took a long time.

The algorithm is based on two equations. Equation (1) is applied to each point x_i in the model to determine the neighbourhood size by calculating the average length of the edges connected to it.

$$I_{avg,i} = \frac{1}{N} \sum_{j \in N(i)} \|x_j - x_i\| \quad (1)$$

This point x_i is considered as being part of a sharp edge if it satisfies equation (2).

$$\frac{1}{|k_i|} < \lambda \cdot I_{avg,i} \quad (2)$$

Here $\frac{1}{|k_i|}$ is the minimum curvature radius for point x_i and k_i is the curvature value for that point.

The value of λ should be adjusted according to the density of points in the model and the precision of the results expected. Figure 17 and Figure 16 show a representation of the sharp edges detected using Mean and Gaussian curvature values with several factors (λ); the points considered sharp edges are represented in red. The areas shown are the sutures in the back of the skull and an orbit due to their relevance to this work.

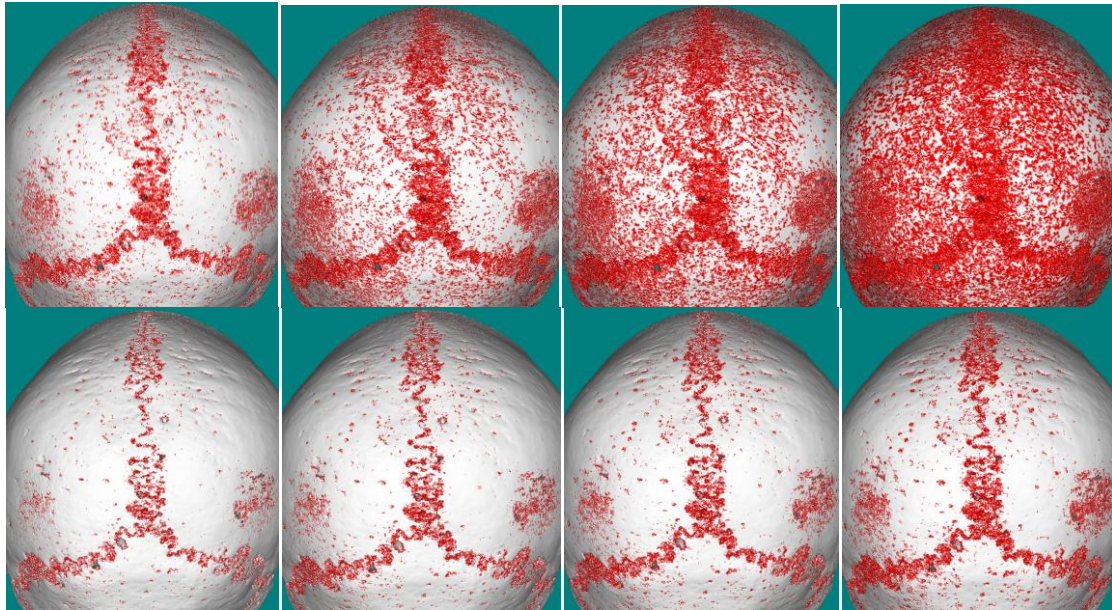


Figure 16 - Sharp edges (in red) detected in sutures using Mean (top) and Gaussian (bottom) curvature values with factors (λ) 14, 25, 35, and 55, from left to right respectively

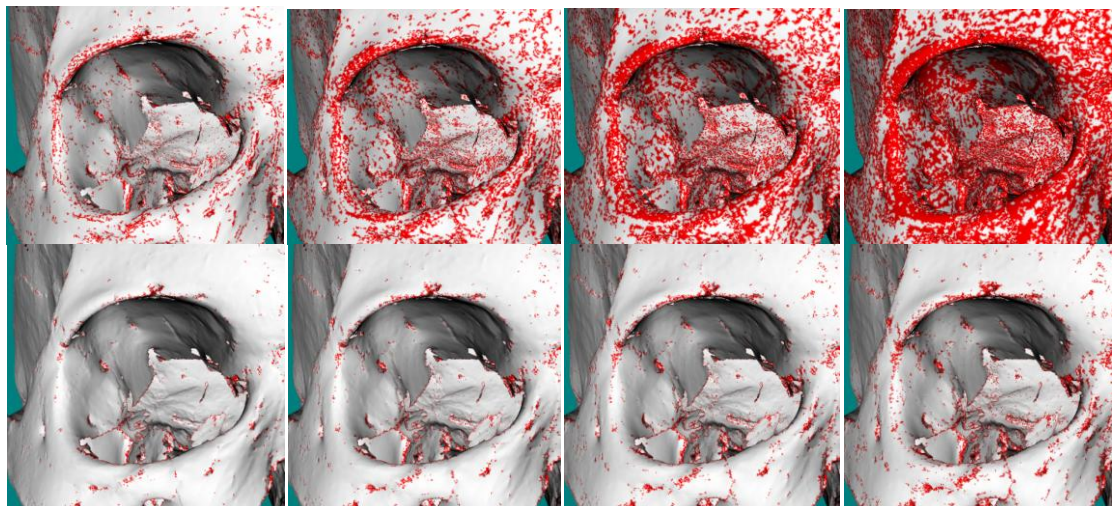


Figure 17 - Sharp edges (in red) detected in an orbit using Mean (top) and Gaussian (bottom) curvature values with factors (λ) 14, 25, 35, and 55, from left to right respectively

4.3 Orbit detection

The methods used to detect the orbit structure (bone cavity in which an eyeball resides) use an interactive approach initially based on seed points picked by the user. Later they were improved to allow the user to guide the structure detection gradually.

4.3.1 Detection using curvature values

A method to detect the orbit using curvature values was implemented. Given three reference points marked by the user, their neighbourhood is analysed and the points with maximum curvature are stored as a structure. Figure 18 shows an example of the structure detected using three reference points in an orbit, in low and high resolution models. The colours of the spheres represent the order in which the structure was found (from darker to lighter).

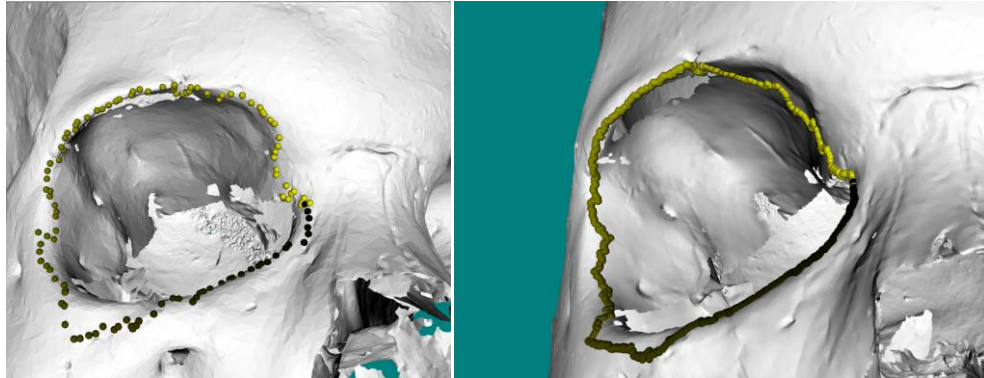


Figure 18 - Example of structure detected between 3 points in an orbit, in low and high resolution models respectively. The colour pattern of the spheres indicates the order in which it was found (darker to lighter)

4.3.2 Detection using Sharp Edges

A method to detect relevant structures using sharp edges was implemented to refine the initial guess provided using the method presented in 4.3.1. The number of reference points was increased due to the results obtained with the previous method in which some sections of the orbit were not being properly detected (as shown in Figure 18 on the top right corner of the orbit to the left). Given four reference points marked by the user, their neighbourhood is analysed and the points considered sharp edges are stored as a structure. The order in which the reference points are marked impacts the result since the algorithm follows the same order when trying to close the structure (connecting the last marked point with the first one). Figure 19 shows an example of the structure detected. The reference points are represented as green spheres and were marked clockwise from the top left to the bottom left. Since the algorithm tries to find the best path between two points. In each iteration, the order in which the points were marked is represented by the colour pattern of the structure. This pattern starts from a black sphere and ends with a magenta sphere, this indicates the order in which the structure was found.

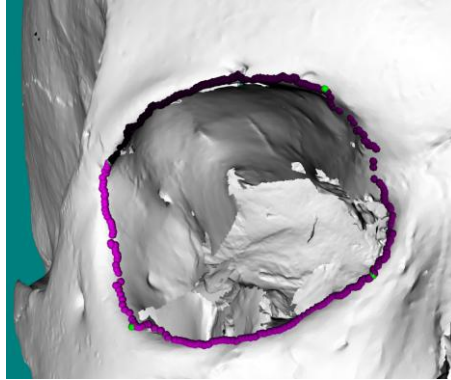


Figure 19 - Structure detected using sharp edges. The four reference points are coloured as green. The colour pattern of the spheres indicates the order in which it was found (darker to lighter)

After consulting the domain experts they mentioned that the main focus of this method should be the 2D shape of the orbit. So, after extracting the structure, the plane that best fits the whole set of points is computed. This was accomplished by using a least squares plane fit method from the *Wild Magic* library (Eberly, n.d.). Shown in Figure 20 is an example of a plane.

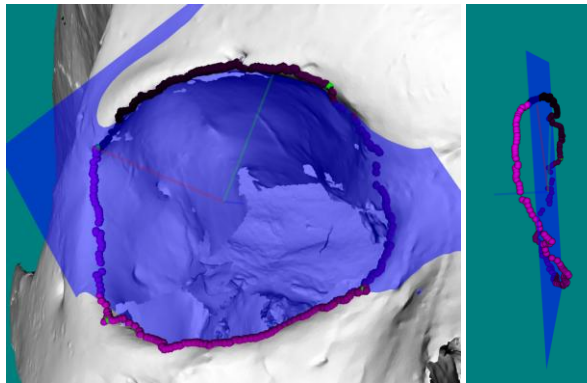


Figure 20 - Plane fitted to the structure. Frontal view (left) and side view (right)

Upon defining the plane, the structure points are projected onto it in order to get a 2D representation of the structure. Each projection is done by displacing the original point in the direction of the plane's normal, as shown in equation (3).

$$\begin{bmatrix} P'_x \\ P'_y \\ P'_z \end{bmatrix} = \begin{bmatrix} P_x \\ P_y \\ P_z \end{bmatrix} + \begin{bmatrix} N_x \\ N_y \\ N_z \end{bmatrix} \times (-D) \quad (3)$$

Where P' represents the projected point, P represents the point, N is the plane's normal and D is the perpendicular distance from the point to the plane.

Figure 21 shows the resulting points after projecting the structure points onto the plane; the structure points are represented as spheres in shades of magenta and their projections are represented by blue spheres.

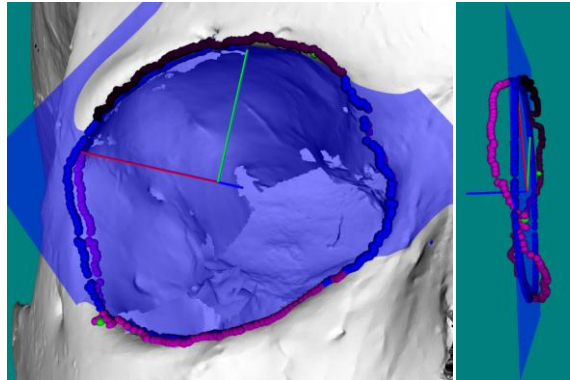


Figure 21 - Structure points projected onto the plane. The projections are represented by blue spheres. Frontal view (left) and side view (right)

Even though all the projected points are situated on the plane, everything is still using a 3D coordinate system. In order to fit an ellipse to the points it is required that they are represented in 2D. For this, a new coordinate system was implemented. The plane's normal vector was used as an axis (blue), another axis was defined from the centre of the set of points to the first projected point (red) and finally the third axis (green) was set perpendicular to the other two. This new coordinate system is shown in Figure 20 and Figure 21 originating from the centre of the set of points. To obtain the 2D coordinates of the projection points, the two vectors that are contained in the plane (red and green) were used as reference. This required a linear system to be solved for each point. Once more, the *Wild Magic* library (Eberly, n.d.) was used to solve the system (using the function `Wm5LinearSystem`). After computing the list of 2D points it was possible to fit an ellipse which minimizes the sum of the distances to all point. The fitting method was done using the *Best-fit* library developed by Alasdair Craig (Craig, 2013). The final result of the fitting is shown in Figure 22. The ellipse points are represented as red spheres and its centre as a white sphere. Its axes are represented as the yellow and light blue line segments. The length of these line segments is used as two of the measures the specialists use, namely OBB and OBH.

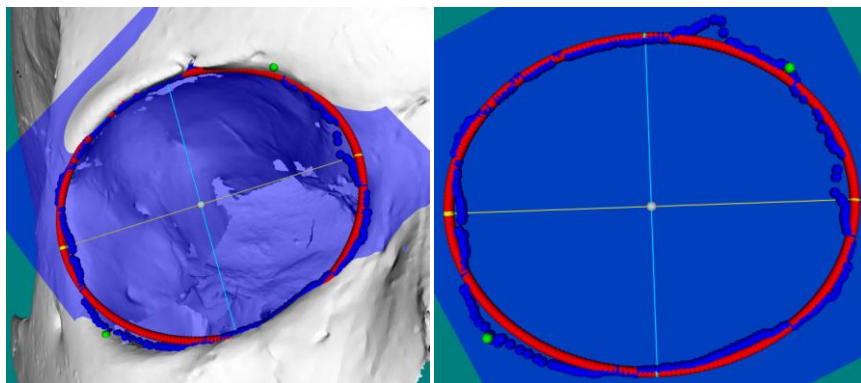


Figure 22 - Ellipse fitted to projected points. Ellipse points are represented as red spheres, the two axis as yellow and light blue. Normal view (left) and view with hidden model (right)

This method was later improved so that the structure would be defined gradually relying on user interaction. The user can mark the reference points gradually and has the option to undo each partial section. The structure is initially defined using two reference points, it then expands incrementally using one additional reference point at a time and finally it tries to close the structure (connecting the last marked reference point to the first one). Figure 23 shows examples of structures detected using three and seven reference points. The reference points are represented as green spheres. The beginning of each section is defined by a black sphere and ends on an orange sphere, indicating the order in which it was found.

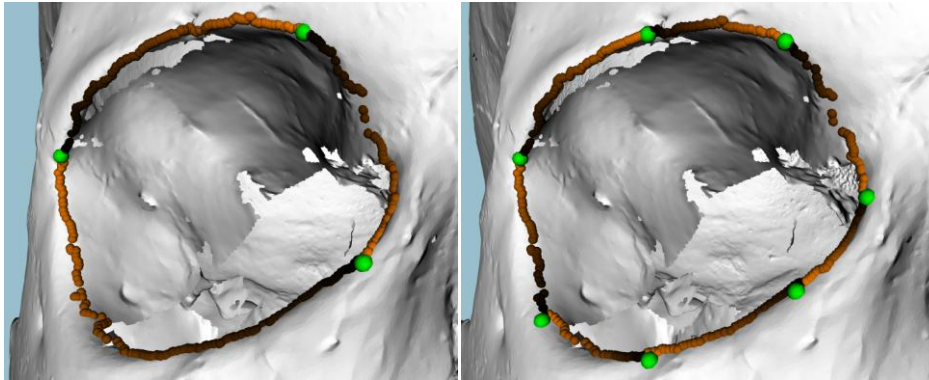


Figure 23 - Structure detected using 3 (left) and 7 (right) reference points. The colour pattern of the spheres indicates the order in which each section was found (darker to lighter)

4.4 Suture detection

This section presents the methods used to detect and classify a suture structure (fibrous joint that binds together skull bones). These methods use two reference points marked by the user and try to find a suture between them. Curvature values were used to obtain preliminary results. Later the sharp edge method was used to detect a suture (Sagittal suture), considered important by the domain experts. Preliminary results on evaluating the complexity of this suture were obtained by comparing the number of points of the model with the number of points detected as part of the suture.

4.4.1 Detection using curvature values

The method to detect sutures using curvature values was implemented as explained in section 4.3.1 but using only two reference points. Figure 24 shows an example of the structures detected in a suture, in low and high resolution models. The colours of the spheres represent the order in which the structure was found (from darker to lighter). As can be seen in the figure this method had its

limitations and so on a second approach the new method based on Sharp Edges was used, as is presented in the next section.

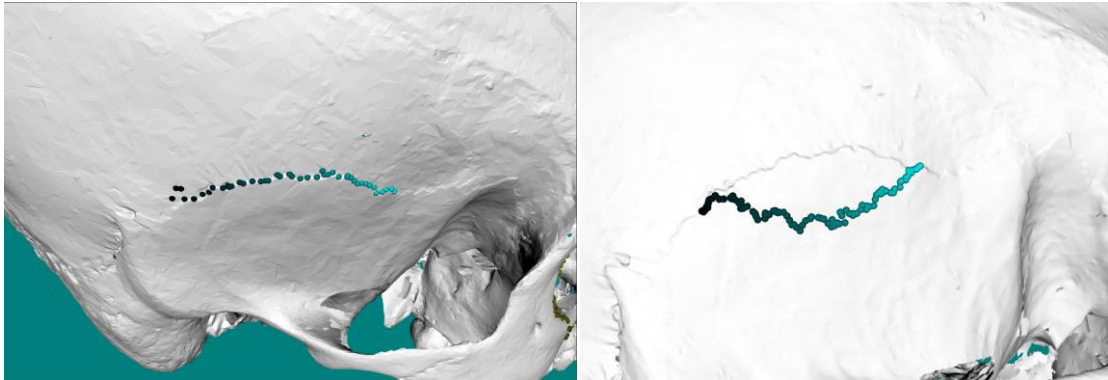


Figure 24 - Example of structure detected between two points in a suture, in low resolution (left) and high resolution (right) models. The colour pattern of the spheres indicates the order in which it was found (darker to lighter)

4.4.2 Detection using Sharp Edges

The method to detect sutures using sharp edges was implemented. It requires two reference points at the extremities of the suture under study to be marked by the user. The algorithm starts by finding a structure composed of sharp edges which defines a direct path connecting the two reference points. Using this structure as a starting point the first neighbourhood level (points directly connected) of each point is analysed in search of more sharp edges. This process is then repeated for each of the new sharp edges found. When no more sharp edges are found or when a neighbourhood threshold is reached (defined by the author) the process stops and computes the results. These results are obtained through the division of the number of sharp edges detected as part of the suture by the total number of points in the model. Since many of the sutures intersect, in order to prevent the detection of sharp edges from another suture a restriction was included in the selection process. The restriction guarantees that the sharp edges used are located between the two reference points. This is done by measuring the distance between the two reference points and discarding any points that are further away from any of the reference points than that distance. Figure 25 shows an example of this method applied to the Sagittal suture (of specimen number 25). The initial structure is represented as blue spheres where the colour pattern indicates the order in which it was found (darker to lighter). Teal spheres represent the sharp edge points detected and considered to be part of the suture.

It is important to mention that this method was just the initial attempt to address the suture classification and still has some issues. For example, in some cases it detects additional portions of the

model as part of the suture (valleys or holes nearby) and in other cases it ignores certain portions of the suture (due to discontinuities or the lack of depth of the suture valley).

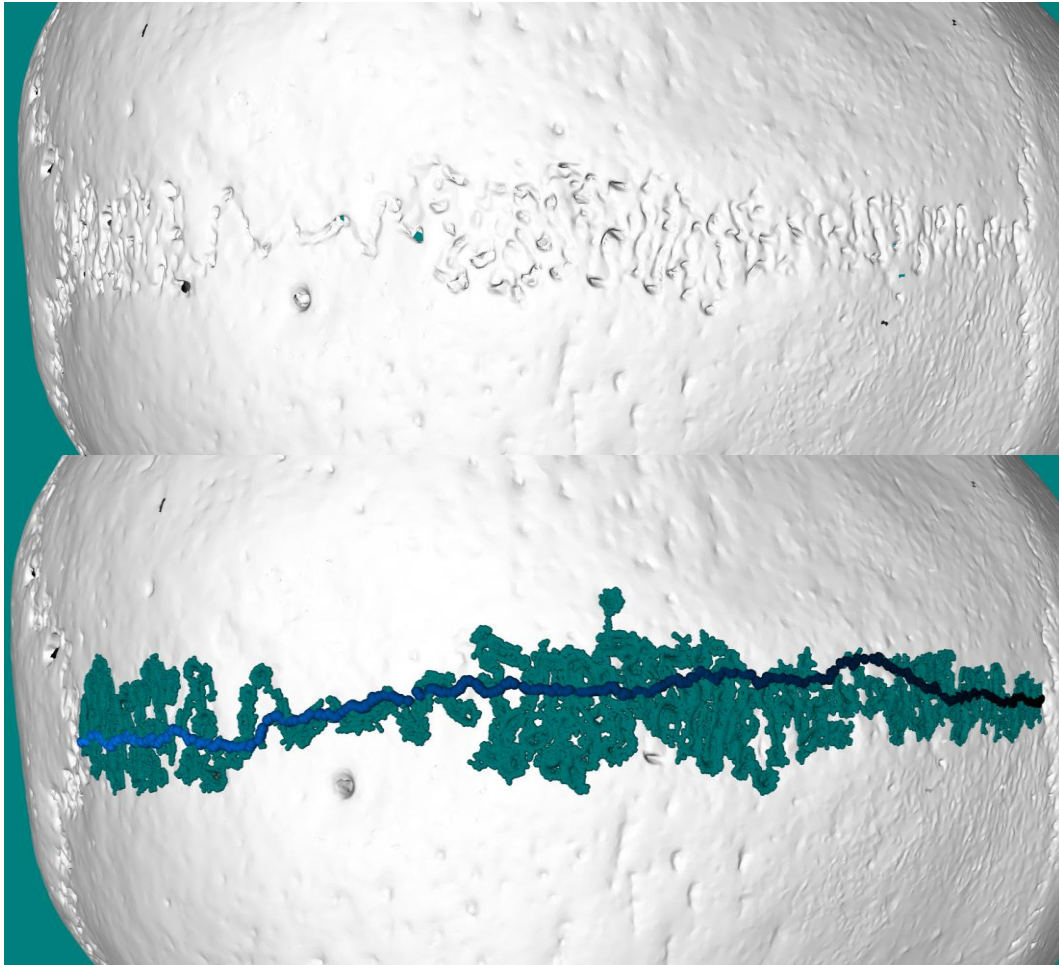


Figure 25 - Example of suture detection on the Sagittal suture. Before (top) and after (bottom) the method is applied. The main structure is represented as blue spheres and the colour pattern indicates the order in which it was found (darker to lighter). Teal spheres represent the points considered to be part of the suture

5 Results

5.1 Overview

This chapter presents and discusses the results obtained throughout this work following the same order as the sections presented above. Firstly, the measures of two skulls taken with the improved CraMs application and with traditional methods are compared. Then, the results from the variability and error analysis of measures by two domain experts using the same methods are compared. Next, the preliminary results concerning the influence of using decimated models on fully automatic measures are presented. These results may open the possibility of using decimated models (much easier to handle) while keeping measures accuracy within a reasonable value. After that, some results concerning the measures obtained using the structure detection method based on sharp edges detection and ellipse fitting are presented and evaluated. Finally, preliminary results obtained with the suture detection method are presented and discussed.

5.2 Craniometric Results and Discussion

Table 7 presents the measures taken by two domain experts using CraMs (App), and traditional methods (Antr) on two of the eight specimens (number 25 and 67) which had the most measures available. Other specimens had fewer measures taken due to fractures. Measurements with the value β (highlighted in bold) were considered to be difficult to obtain by the experts for that specific specimen and therefore were ignored. Results for all specimens can be found in Appendix C.

The table is divided into three sections to differentiate the three types of measures provided in the application: measures done using two Automatic points as green, measures that use at least one Semi-Automatic point (these are points detected with user intervention) as blue, and measures that use only Manual points (defined solely by the user) as orange.

	Specimen #25				Specimen #67			
	User #1		User #2		User #1		User #2	
	App	Antr	App	Antr	App	Antr	App	Antr
1 - ZYB	136,7	136	136,7	137	126,5	126	126,5	126
2 - BBH	142,7	142	142,7	143	131	131	131	130
3 - XCB	135	131	135	131	131,5	122	131,5	126
4 - GOL	182,1	181	182,1	181	182	182	182	173
5 - BNL	105,3	106	105,3	107	104,6	104	104,6	105
6 - FRC	116,6	114	116,6	115	109,6	107	109,6	108
7 - BPL	102,8	103	102,8	104	100	94	100,7	102
8 - UFHT	64,6	62	64,8	64	63,4	64	65,6	66
9 - MAB	65,3	66	65,7	65	60,1	61	59,1	61
10 - AUB	116,9	110	114,6	108	110,4	107	107,7	107
11 - NLH	48,5	47	48,5	46	49,6	49	49,2	49
12 - UFBR	106,7	106	106,7	109	105,2	106	105,3	108
13 - PAC	115,3	115	114,7	116	105,5	106	105,9	105
14 - FOL	40	39	40,8	38	33,3	32	33,6	32
15 - MAL	54,3	56	53	58	54	57	53,6	59
16 - MDH	31,5	31	28,8	32	25,8	27	23,5	25
17 - OBB	44,1	47	42,6	43	46,5	43	46,6	42
18 - OBH	35,3	35	34,9	33	33,8	34	34,2	32
19 - WFB	99,7	101	98,5	101	93,6	96	92,7	95
20 - NLB	27,6	28	28,8	27	26,4	26	27,2	25
21 - EKB	102,4	100	98,9	100	100,8	99	100,5	98
22 - DKB	β	β	β	β	27	27	21	26
23 - OCC	93,6	94	93,5	96	96,7	97	96,3	97
24 - FOB	28,9	29	31,7	29	31,6	30	33,4	30

Table 7 - Measure values for two specimens obtained by two Anthropologists using Crams (App) and traditional methods (Antr). Automatic (green), Semi-Automatic (blue) and Manual (orange)

These results show that the discrepancy between measures obtained with both methods (traditional and CraMs) can be considered within a low threshold, better or similar to the discrepancy between domain experts using the same methods in most cases. To further study these results a couple of analysis were performed, which are presented in the next section.

5.2.1 Inter-Observer variability and error analysis

In order to better validate the results obtained using CraMs further analyses were performed. The variability in measures was calculated (difference between measures) and the error margin was computed. These methods of analysis are the same as the methods used by domain experts to validate measures in their studies (with traditional methods); therefore calculating them for the measures obtained with CraMs allowed for more coherent comparisons to be made between them.

Figure 26 shows the difference in percentage for each measure taken by both specialists, using CraMs and Traditional methods. Mean values are represented as squares, the maximum and minimum values are represented as the limits of the vertical lines. To obtain these results a total of eight specimens were taken into account. It is important to note that not all the measures for all the specimens were available. So, in order to make valid comparisons, the values that were used in the calculations were the ones available from both experts using both methods.

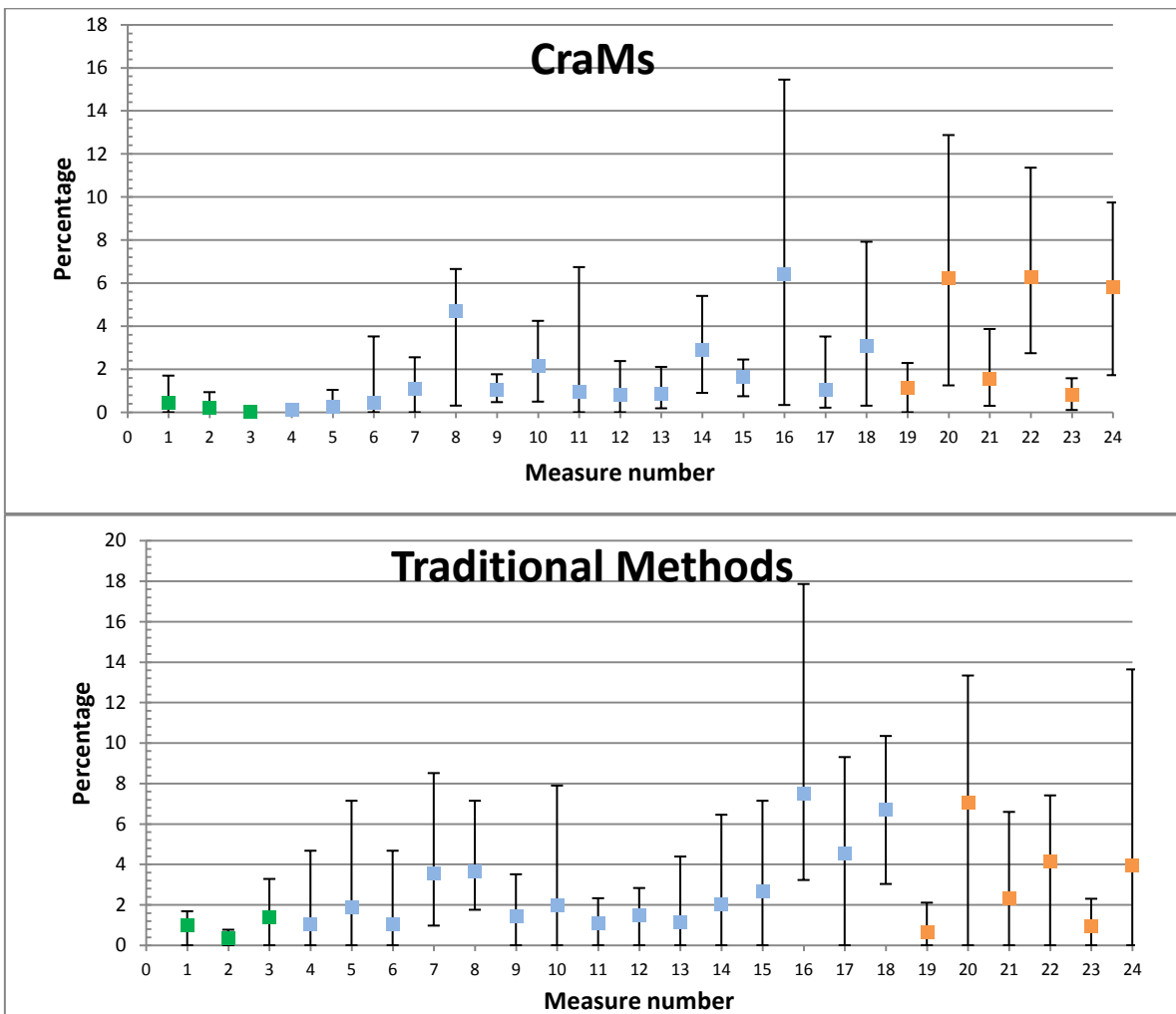


Figure 26 - Bar plots with the difference percentage for each measure between specialists using CraMs (top) and traditional methods (bottom). Automatic (green), Semi-Automatic (blue) and Manual (orange)

These graphics suggest that for automatic measures taken with CraMs the average difference percentage and variations decrease in comparison with the ones taken using traditional methods. It seems that semi-automatic measures also show better results using CraMs. Manual measures show a larger discrepancy due to the fact that they solely depend on points the user picked with no aid from the application. These results become more obvious when analysing the values in Table 8 which show the average difference percentages for each type of measure. Note that the number of measures in parenthesis represents the scenario where all measures are available for all specimens.

Type	App (%)	Antr (%)	Number of Measures
Auto	0,19	0,90	16 (in 24)
Semi-A.	1,86	2,83	109 (in 120)
Manual	3,37	3,06	41 (in 48)

Table 8 - Average difference percentages obtained for each type of measure. Automatic (green), Semi-Automatic (blue) and Manual (orange)

According to (Perini, de Oliveira, Ornelia, & de Oliveira, 2005) a common way to express the error margin in anthropometry is using the technical error of measurements (*TEM*). The value represents the standard deviation between repeated measurements. Through its usage anthropologists are able to quantify the inter- and intra-observer errors. Since the specialists from iDryas adopted this value to validate their measurements using traditional methods it was also used to validate the ones taken with the application. It is calculated by applying equation (4) followed by equation (5).

$$Absolute\ TEM = \sqrt{\frac{\sum d_i^2}{2n}} \quad (4)$$

$$Relative\ TEM = \frac{Absolute\ TEM}{VAV} * 100 \quad (5)$$

Where *d* = measures deviation

n = number of measures

i = index of the measure

TEM = Technical error of measurement (expressed in percentage)

VAV = Variable average (average of the average between all the observations, for each measure).

TEM values may vary within a scale of 0 to 100%. Typically a value above 10% means the measures are not acceptable when comparing inter-observer measures. Analysing TEM values shown in Table 9 for CraMs (App) suggests that the more automated the process of selection is the better the results are. Through the comparison of the TEM values for the same measures taken with CraMs and with traditional methods, it is clear that the application has potential to be more reliable than the traditional methods for taking measures in terms of consistency and repeatability.

Type	App (%)	Antr (%)	Number of Measures (%)
Auto	0,30	0,88	67
Semi-A.	1,39	2,35	91
Manual	1,74	1,99	85

Table 9 - TEM values obtained for each type of measure. Automatic (green), Semi-Automatic (blue) and Manual (orange)

5.3 Decimation Results and Discussion

As explained in section 3.2.5 a preliminary study on the impact decimation has on measures was conducted. The results in Table 10 and Table 11 show the values for three measures obtained on two specimens with different decimation levels (further results are presented in Appendix D). Only automatic measures were used since the error in manual and semi-automatic measures is influenced by user interaction. All eight models were used in this study but results here only consider two models, those that are in better condition to obtain the three automatic measures. A more extensive study was done on models #25 and #65, the idea was to investigate the existence of a "breaking point" in which the error in measures might suddenly become unacceptable. This was the case for the measure XCB on model #65 and BBH on both models at 1%, which is why these were not used and are highlighted as bold.

	Specimen #25								
	100%	80%	60%	40%	20%	10%	5%	2,5%	1%
ZYB	136,70	136,73	136,73	136,73	136,74	136,75	136,74	136,71	137,25
BBH	142,70	142,70	142,70	142,70	142,70	142,72	142,71	142,71	57,19
XCB	135,00	135,03	135,03	135,03	135,04	136,66	135,04	136,44	135,61

Table 10 - Automatic measures taken on model #25 with different degrees of decimation. The percentage indicates the number of vertices in the model compared to the original

	Specimen #65								
	100%	80%	60%	40%	20%	10%	5%	2,5%	1%
ZYB	136,17	136,17	136,17	136,16	136,17	136,17	136,20	136,32	136,35
BBH	140,15	140,18	140,16	140,17	140,16	140,13	139,97	138,54	102,61
XCB	130,25	130,26	130,26	130,27	130,26	130,24	130,21	130,09	146,19

Table 11 - Automatic measures taken on model #65 with different degrees of decimation. The percentage indicates the number of vertices in the model compared to the original

To better analyse these measures the differences between the original and decimated models were calculated in percentage for each measure. The final results presented in Figure 27 indicate the percentage of the average differences related to the original measurement. It seems clear that,

given the high resolution of the original model, even using a model that has only 40% of the original vertices seems to have little or no effect on the obtained measures. This means that the performance of CraMs can be significantly improved on machines with low computational resources, which is often the case for most specialists' personal or work computers.

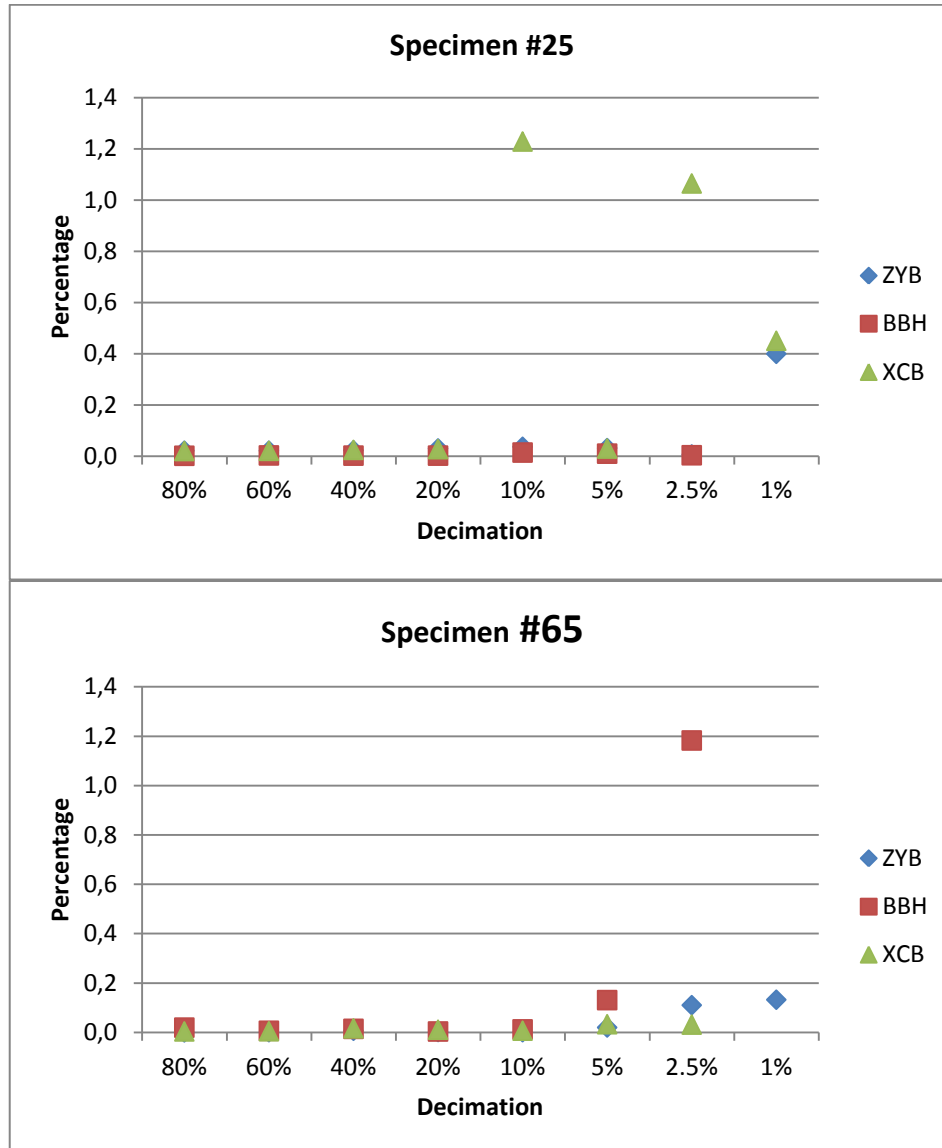


Figure 27 - Graphics with the difference percentages in relation with the original models. Model #25 (top) and Model #65 (bottom)

5.4 Orbit detection Results and Discussion

This section presents some results regarding the orbit detection (see section 4.3.2). Table 12 shows the measures extracted from the ellipse fitting algorithm (App) and the ones taken by the anthro-

pologists using traditional methods (Antr) from three of the eight specimens (consult Appendix C for all the results). In order to extract the measures from the ellipse the length of its two axes is measured. The length of the major axis is used as the measure OBB and the length of the minor axis is used as the measure OBH. The comparison with the measures obtained using traditional methods presents a small discrepancy suggesting that this is a valid approach. It is noteworthy that specialists mentioned that these two measurements are difficult to perform using traditional methods resulting in a significant variability in the values obtained. The main constraint is that the OBH measurement must be done as if it was perpendicular to the OBB measurement which is difficult to do accurately by hand. This constraint is much easier to ensure in a computer application using an ellipse fitting algorithm since it is guaranteed that both axes are perpendicular.

Measure	Specimen #57				Specimen #65				Specimen #67			
	User #1		User #2		User #1		User #2		User #1		User #2	
	App	Antr	App	Antr	App	Antr	App	Antr	App	Antr	App	Antr
OBB	42,7	43	43	43	43,2	43	42,9	42	46,5	43	46,6	42
OBH	32,8	33	32,7	32	33,8	34	33,2	33	33,8	34	34,2	32

Table 12 - Measures obtained by two Anthropologists using the orbit detection method (App) and traditional methods (Antr)

These results were already taken into consideration in the previous bar plot (Figure 26). Figure 28 shows a bar plot focused on the two measures being analysed here. It shows the difference percentages for these two measures taken by the domain experts using both methods. Mean values are represented as squares, the maximum and minimum values are represented as the limits of the vertical lines. Comparing the two methods, there appears to be a decrease in the average and limit percentages using CraMs. With further analysis of the results shown in Table 13, which shows the TEM values (explained in section 5.2.1) obtained for the two measures, the reduction in variability becomes clear.

Type	App (%)	Antr (%)	Number of Measures (%)
OBB	1,01	3,77	100
OBH	3,17	4,84	100

Table 13 - TEM values obtained for the two measures OBH and OBB

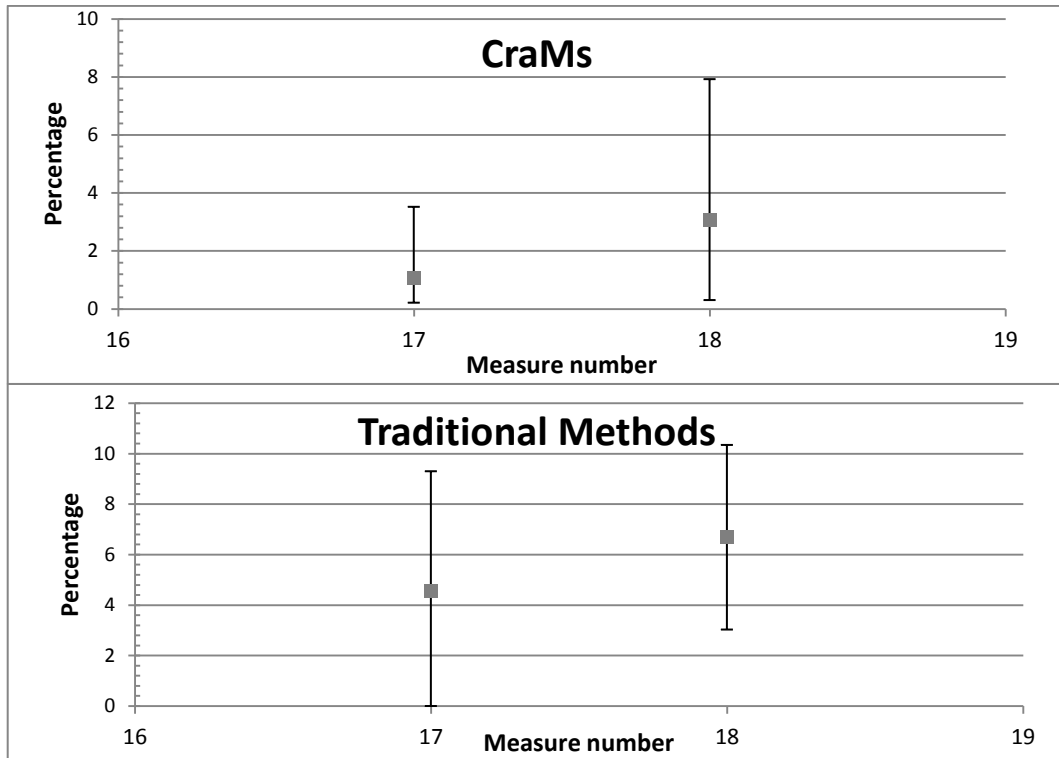


Figure 28 - Bar plots with the difference percentage for two measures between specialists using CraMs (top) and traditional methods (bottom). OBB (number 17) and OBH (number 18)

Since the OBB measure is obtained using two reference points (Dakyon and Ektokonchion) and since there are two additional measures that use these points (EKB between the two Ektokonchions and DKB between the two Dakyons) a question arose. Whether or not the points defined by the orbit detection method (used to obtain OBB) could be used for these two measures (EKB and DKB). In search of an answer the two orbits were detected in all eight specimens and these measures were obtained. Table 14 shows the results obtained for three of the eight specimens by the author with the orbit detection method (App) and by the two domain experts using traditional methods (Antr), see Appendix E for all results. Measurements with the value β (highlighted in bold) were considered to be difficult to obtain by the experts for that specific specimen.

Measure	Specimen #65			Specimen #66			Specimen #67		
	App	Antr #1	Antr #2	App	Antr #1	Antr #2	App	Antr #1	Antr #2
OBB	42,4	43	42	41,5	42	43	43,4	43	42
OBH	32,8	34	33	31,6	32	30	33,5	34	32
EKB	107	100	97	101	95	96	104	99	98
DKB	27,5	β	β	23,9	27	29	23,1	27	26

Table 14 - Measures obtained from the orbit detection method.

Results obtained for the measures EKB and DKB with the application show a significant discrepancy with the ones obtained with traditional methods. This can be attributed to the fact that in most

cases the points defined by the orbit detection method are not part the model and that their alignment does not accurately represent the orientation in which the traditional measurements are taken. If these issues are addressed the orbit detection method can be used to obtain four measures correctly (instead of just two).

5.5 Suture detection Results and Discussion

This section presents the preliminary results obtained with the suture detection method (see section 4.4.2). The complexity of a suture can be classified as being simple, complex or intermediate. The following results were obtained concerning the Sagittal suture. Unfortunately, the domain experts have not yet provided with their classifications. So, the ones presented here were done by the author of this work through a visual analysis of the skull models. The classification process can be very difficult depending on the baseline used. Figure 29 shows the Sagittal suture on three of the eight skulls (numbers 65, 21 and 25 from top to bottom); the different classifications were attributed by the author (consult Appendix F for the figures on all skulls).

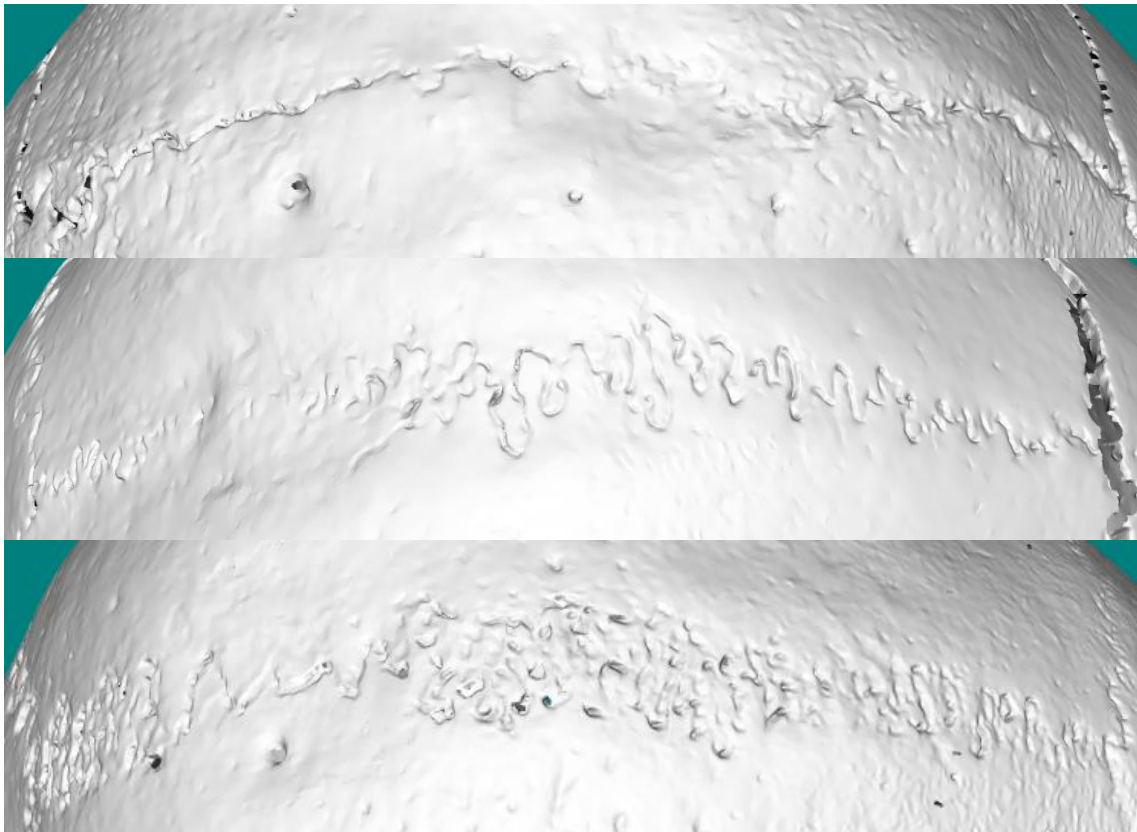


Figure 29 - Example of Sagittal suture on three skulls (65, 21 and 25) with different complexity classifications. The classifications given to these by the author are: Simple (top), Intermediate (middle) and Complex (bottom),

Table 15 shows the results of this preliminary study concerning the Sagittal suture in all eight specimens. It is important to mention that in some cases (specimen 65, 66 and 67) the detection method could not detect certain portions of the suture due to their depth being too similar to their surroundings or due to some discontinuities in the suture valley, these results were highlighted in bold since they still need improvements.

Specimen	Classification	Points in model	Suture points	Ratio (%)
#21	Intermediate	1.370.198	17.787	1,30
#25	Complex	1.512.605	46.645	3,08
#38	Simple	1.801.451	6.869	0,38
#39	Intermediate	1.849.701	35.778	1,93
#57	Intermediate	2.096.164	35.128	1,68
#65	Simple	1.711.944	18.280	1,07
#66	Intermediate	2.440.999	22.428	0,92
#67	Intermediate	2.229.845	24.609	1,10

Table 15 - Results from the suture detection method for all eight specimens. The ratio is the percentage of suture points compared to the total points in the model

Ignoring the specimens which had detection issues (highlighted in bold), the ratios obtained seem to show some correlation with the classifications, with higher values representing higher suture complexity. This method is just a first approach and needs further investigation, but it already provided some interesting results. With additional research and refinement the suture detection method might provide valid results for future craniometric studies.

6 Conclusion and Future Work

6.1 Conclusion

CraMs proposes an alternative way for anthropologists to take specimen measurements, making them more consistent and ensuring a better preservation of the specimen by avoiding physical manipulation and transportation. A new version, more usable, more reliable and including more measures, was developed in this work.

Measures taken with CraMs can be classified in three major categories: Automatic, Semi-Automatic and Manual. From the twenty four measurements that anthropologists typically use, CraMs can be used to take all of them, three fully Automatic, fifteen Semi-Automatic and six Manual.

Even though the study on decimation and its impact on the measures was preliminary it provided useful information. The fact that the domain experts can use models with half the resolution and have little or no error induced from it is really interesting. By reducing the complexity of the model without affecting the measures, the flow of interaction of the user with the application will improve significantly.

In terms of the sharp edge methods the results obtained so far were very positive. The fact that two measures difficult to obtain with traditional methods can be extracted almost automatically with the orbit detection method is a significant improvement. Concerning the detection and classification of sutures it seems that valid results can be achieved with further research and development of the method presented. These tools may be extremely useful for the anthropologists in their future studies.

All the results obtained so far are very positive and begin to show the potential of CraMs and the application of new technologies in the field of Anthropology.

6.2 Future Work

CraMs still has a lot of room to improve and expand. There is still a vast number of technologies and methods that have not been explored. Future work in this project might involve:

- Developing methods to increase the number of points detected automatically (using for example texture information available from the acquisition process) and better support for user interaction (for example using force feedback devices to ease point selection);
- Other feature analysis and classification methods can be tested to improve accuracy, robustness or speed (given the need for user interaction) using for example segmentation, shape analysis, volume analysis, etc.;
- Another idea worth investigating once a significant database of point coordinates is available is to use these coordinates to suggest where the relevant points should be located. These suggested points could be used as seed points instead of the current process of manual picking performed by the user;
- Improving the ICP alignment method by using a database of template models, already aligned, and choosing the most anatomically similar one to obtain the best alignment results;
- Develop a method to automatically align the models. Even though the ICP method works well it might still need user interaction in some cases;
- Since some of the models are fragmented, a method to help align fragments and reconstruct the mesh in the missing areas would be of great use;
- Improving the sharp edge structure detection methods in order to make them automatic and more accurate;
- Optimization was not considered as a priority during the work developed here. This means the amount of resources needed to perform certain tasks might be at a high level. This will eventually become a problem since user interaction is a significant part of this project and thus improvements in this respect are important.

References

- An, Y., Li, Z., & Shao, C. (2013). Feature Extraction from 3D Point Cloud Data Based on Discrete Curves. *Mathematical Problems in Engineering*, 2013, 1–19.
- Balzeau, A., Crevecoeur, I., Rougier, H., Froment, A., Gilissen, E., Grimaud-Hervé, D., ... Semal, P. (2010). Applications of imaging methodologies to paleoanthropology: Beneficial results relating to the preservation, management and development of collections. *Comptes Rendus Palevol*, 9(6-7), 265–275.
- Baylac, M., & Friess, M. (2005). Fourier Descriptors , Procrustes Superimposition , and Data Dimensionality: An Example of Cranial Human Populations. *Modern Morphometrics in Physical Anthropology*, 145–165.
- Besl, P. J., & McKay, H. D. (1992). A method for registration of 3-D shapes. *IEEE Transactions on Pattern Analysis and Machine Intelligence*, 14(2), 239–256.
- Blakey, M. L. (2001). Bioarchaeology of the African diaspora in the Americas: Its origins and scope. *Annual Review in Anthropology*, 30, 387–422.
- Buck, T. J., & Vidarsdottir, U. S. (2004). A proposed method for the identification of race in sub-adult skeletons: a geometric morphometric analysis of mandibular morphology. *Journal of Forensic Sciences*, 49, 1159–1164.
- Coelho, C. R. S. (2012). Uma identidade perdida no mar e reencontrada nos ossos: Avaliação das afinidades populacionais de uma amostra de escravos dos séculos XV-XVI. *Master Dissertation, University of Coimbra*.
- Craig, A. (2013). Best-fitting line, circle and ellipse. Retrieved May 12, 2014, from <http://www.codeproject.com/Articles/692787/Best-fitting-line-circle-and-ellipse>
- Eberly, D. (n.d.). Geometric Tools. Retrieved March 31, 2014, from <http://www.geometrictools.com>
- Gahm, G. (2010). Mesh decimation. *Computing*, 1–6.
- Garland, M., & Heckbert, P. S. (1997). Surface simplification using quadric error metrics. *Proceedings of the 24th Annual Conference on Computer Graphics and Interactive Techniques - SIGGRAPH '97*, 209–216.
- Gonzalez, P. N., Bernal, V., & Perez, S. I. (2011). Analysis of sexual dimorphism of craniofacial traits using geometric morphometric techniques. *International Journal of Osteoarchaeology*, 21, 82–91.
- Gumhold, S., Macleod, R., & Wang, X. (2001). Feature Extraction from Point Clouds. *In Proceedings of the 10 Th International Meshing Roundtable*, 293–305.

- Hefner, J. T. (2009). Cranial nonmetric variation and estimating ancestry*. *Journal of Forensic Sciences*, 54, 985–995.
- Howells W., W. (1973). Cranial Variation in Man - A Study by Multivariate Analysis of Patterns of Difference among Recent Human Populations. *Papers of the Peabody Museum of Archaeology and Ethnology*, (67), 1–259.
- Lai, Y.-K., Zhou, Q.-Y., Hu, S.-M., Wallner, J., & Pottmann, H. (2007). Robust feature classification and editing. *IEEE Transactions on Visualization and Computer Graphics*, 13(1), 34–45.
- Li, J., & Fan, H. (2013). Curvature-direction measures for 3D feature detection. *Science China Information Sciences*, 56(9), 1–9.
- Meshlab. (2014). Visual Computing Lab - ISTI - CNR. Retrieved from <http://meshlab.sourceforge.net/>
- Neves, M., Almeida, M., & Ferreira, M. (2010). Separados da vida e na morte: retrato do tratamento mortuário dado aos escravos africanos na cidade moderna de Lagos. 7º encontro de arqueologia do algarve. *XELB 10*, 547–560.
- Neves, M., Almeida, M., & Ferreira, M. (2011). História de um arrabalde durante os séculos xv e xvi: o “poço dos negros” em Lagos (algarve, Portugal) e o seu contributo para o estudo dos escravos africanos em Portugal. *Câmara Municipal de Lagos*, 29–46.
- Pauly, M., Keiser, R., & Gross, M. (2003). Multi-scale Feature Extraction on Point-Sampled Surfaces. *Computer Graphics Forum*, 22, 281–289.
- Pereira, C. B., & De Mello E Alvim, M. C. (1979). Manual Para Estudos Craniométricos E Cranioscópicos. *Univ. Federal de Santa Maria*.
- Perini, T. A., de Oliveira, G. L., Ornelia, J. S., & de Oliveira, F. P. (2005). Technical error of measurement in anthropometry. *Revista Brasileira de Medicina Do Esporte*, 11, 81–85.
- Ross, A. H., Ph, D., Slice, D. E., & Williams, S. E. (2010). Geometric Morphometric Tools for the Classification of Human Skulls.
- Santos, D. (2013). 3D skull models: a new craniometric approach. *Master Dissertation, University of Aveiro*.
- Sholts, S. B., Walker, P. L., Kuzminsky, S. C., Miller, K. W. P., & Wärmländer, S. K. T. S. (2011). Identification of group affinity from cross-sectional contours of the human midfacial skeleton using digital morphometrics and 3D laser scanning technology. *Journal of Forensic Sciences*, 56(2), 333–8.
- Sholts, S., Walker, P. L., Miller, K., & Wärmländer, S. (2007). The application of three-dimensional midfacial profiling in the identification of human skeletal remains. *International Symposium on Human Identification Los Angeles, California, October 2, 2007*, 1–10.

- Stephens, C. (2000). A Measure of Truth? An Examination of the History , Methodology , Theory and Practice of Craniometric Analysis: With Special Focus on its Application in Forensic Identification. *Totem: The University of Western Ontario Journal of Anthropology*, 8.
- Vieira, M., & Shimada, K. (2005). Surface mesh segmentation and smooth surface extraction through region growing. *Computer Aided Geometric Design*, 22, 771–792.
- Vioarsdóttir, U. S., O'Higgins, P., & Stringer, C. (2002). A geometric morphometric study of regional differences in the ontogeny of the modern human facial skeleton. *Journal of Anatomy*, 201(3), 211–29.
- Wachowiak, M. J., & Karas, B. V. (2009). 3D Scanning And Replication for Museum AND Cultural Heritage Applications. *Journal of the American Institute for Conservation*, 48, 141–158.
- Watanabe, K., & Belyaev, A. (2001). Detection of salient curvature features on polygonal surfaces. *Computer Graphics Forum*, 20(3).
- Weber, G. W. (2013). Another link between archaeology and anthropology: Virtual anthropology. *Digital Applications in Archaeology and Cultural Heritage*, 1(1), 3–11.

Appendix A – Points of Interest

All figures shown in this appendix were taken from (Pereira & De Mello E Alvim, 1979). The following points were defined as being feature points to use in the classification of the skulls:

1. Alveolon (alv): intersection point of the mid line of the palate with the perpendicular tangent to the posterior border of the alveolar arch;

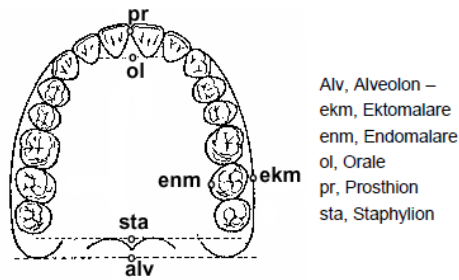
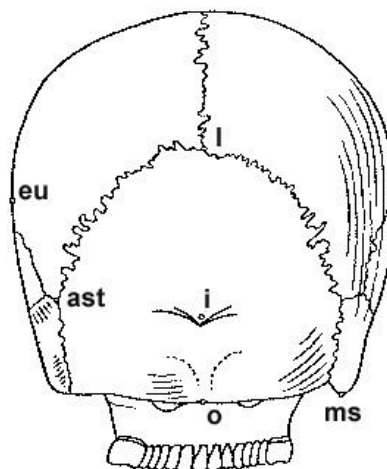


Figure 1 - Palatal arch

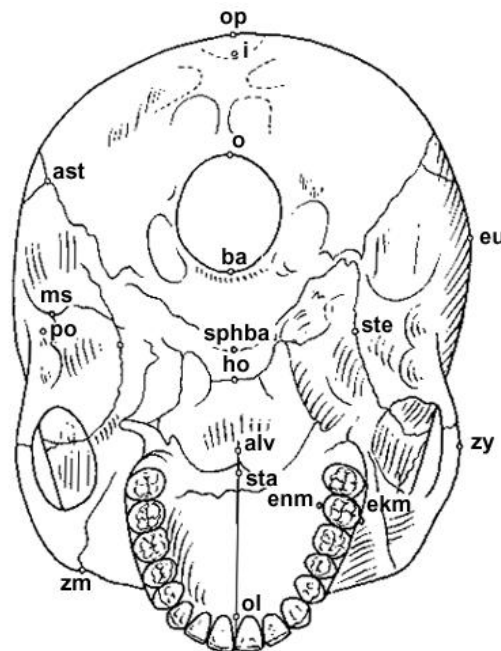
2. Basion (ba): the point is situated on middle border of the anterior margin of the foramen magnum. This feature point is defined as the point with minimum Y coordinate in the Z axis (considering a threshold of ± 0.01 mm in X and ± 10 mm in Z coordinates);
3. Bregma (b): intersection point between the sagittal suture and the coronal suture. The algorithm selects a starting point as the coordinate with greater Y value on the region of points of X and Z within a ± 0.01 mm threshold. Then, it analyses neighbour points in order to find a discontinuity in the Y values, i.e., sudden smaller followed by higher Y values with the aim of finding the coronal suture. Once the suture region is found, the Bregma is selected as point in the region with smaller Y coordinate;



Ast, Asterion – eu, Eurion – i, Inion – lambda, Lambda – mas, Mastoidale – o, Opisthion.

Figure 2 - Skull back view

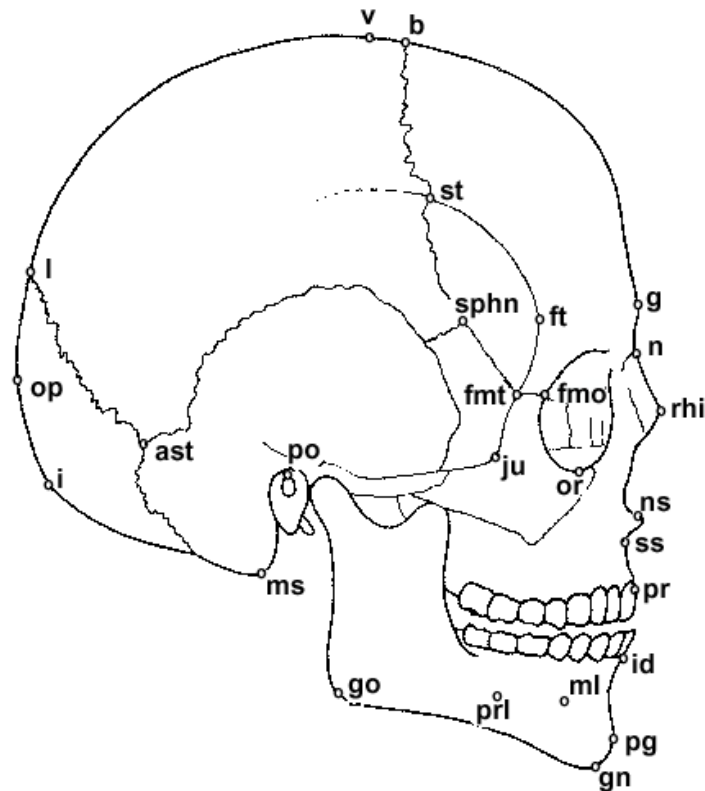
4. Dakyon (d): point located at the apex of the angle formed by the frontolacrimal suture and lacrimomaxilar suture;
5. Ektokonchion (ek): Point located on the outer edge of the orbit and the furthest possible of the *maxillofrontale* point;
6. Ektomalare (ekm): Point situated in the palatal surface of the alveolar arch, in the middle portion of the second molar;
7. Eurion (eu): Most lateral point of the *neurocranium*. Has no fixed location and varies from one individual to another and from one population to another;
8. Frontotemporale (ft): most anterior point of the temporal line, located approximately at the root of the zygomatic apophysis of the frontal bone;
9. Frontomolare-Temporale (fmt): point most posterior and lateral of the frontomalar suture, in the temporal region;
10. Glabella (g): Point located just above the frontonasal suture, between the superciliary arches. Commonly is the most salient point of the front, in the sagittal plane. It may, however, constitute or form a depression, with the superciliary arch (a single continuous elevation);



alv, Alveolon - ast, Asterion - ba, Basion - ekm, Ektomalare - enm, Endonmlare - eu, Eurion - ho, Hormion - i, Inion - ms, Mastoideale - o, Opisthion - op, Opisthokranion - ol, Orale - po, Porion - sphba, Sphenobasion - sta, Staphylion - ste, Stenion - zy, Zygion - zm, Zygomaxillare.

Figure 3 - Skull bottom view

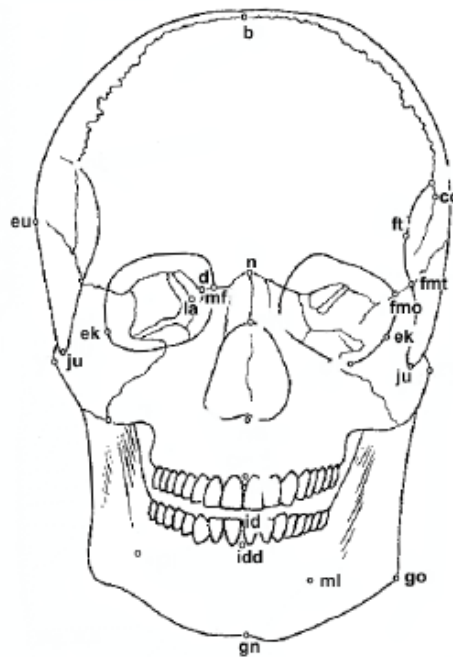
11. Lambda (l): Intersection point between the sagittal and lambdoid sutures;
12. Mastoidale (ms): Lowest point of the mastoid process of the temporal;
13. Nasion (n): Intersection point of the frontonasal suture and suture internasal. Corresponds to the root of the nose;
14. Nasospinale (ns): Lowest point in the inferior edge of the piriform aperture at the base of the nasal spine, designed in the Sagittal Plane. This point is called by some authors Subnasale or Nasale;
15. Opisthion (o): Mid point of the posterior edge of the occipital hole;
16. Opisthokranion (op): Point that is the furthest from the *glabella* in sagittal plane of the occipital. Sometimes coincides with the *inion*. There are cases where this occipital region is more or less flat;



ast, Asterion – b, Bregma – fmo, Frontomalare orbitale – fnt, Frontomale temporale – ft, Frontotemporale – g, Glabella – gn, Gnathion – go, Gonion – i, Inion – id, Infradentale – ju, Jugale – l, Lambda – ms, Mastoidale – ml, Mentale – n, Nasion – ns, Nasospinale – op, Opisthokranion – or, Orbitale – pg, Pogonion – po, Porion – prl, Prominentia laterale – pr, Prosthion – rhi, Rhinion – sphn, Sphenion – st, Stephanion – ss, Subspinale – v, Vertex

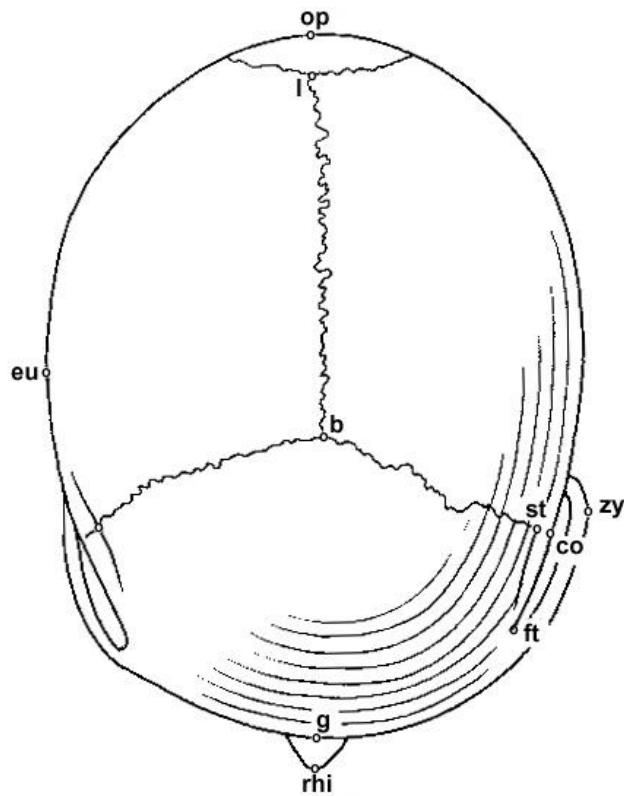
Figure 4 - Skull side view

17. Porion (po): Point on the upper and outer border of the external auditory canal;
18. Prosthion (pr): Most anterior point of the alveolar ridge between the central incisors. Corresponds to the lower end and anterior interalveolar septum in the sagittal plane;
19. Vertex (v): Highest point of the skull located in the sagittal suture and in the frankfurt plane;
20. Zygion (zy): Most lateral point of the zygomatic arch, on each side. Given the aligned skull both Zygion are defined as the points with maximum and minimum X coordinates, respectively to the right and left points. Since the zygomatic arch might not be the largest zone of the skull, we only consider the portion of the skull with negative Y values;
21. Zygomaxillare (zm): Lowest point of the maxilomalar suture.



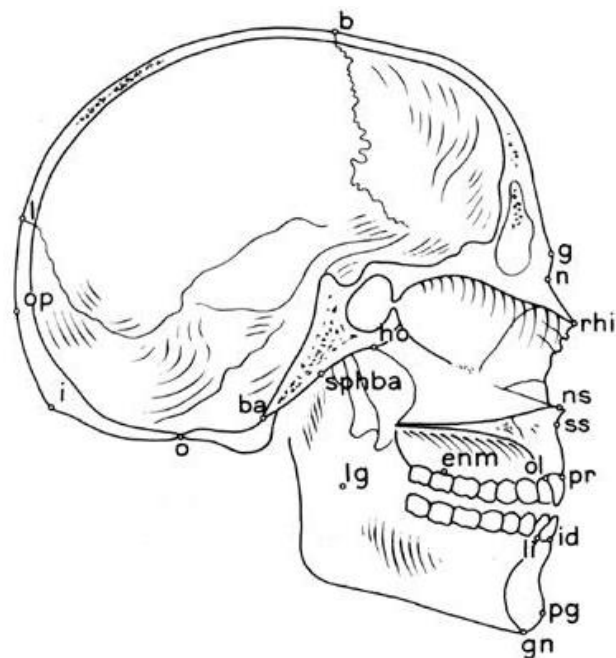
b, Bregma – co, Coronale – d, Dakyon – ek, Ektokonchion – eu, Eurion – fmo, Frontomolare orbitate- fmo, Frontomolare temporale – ft, Frontotemporale – gn, Gnathion – go, Gonion – id, Infradentale – idd, Infradentale dentale – ju, Jugale – la, Lacrimale – mf, Maxillofrontale – ml, Mentale – n, Nasion – ns, Nasospinale – or, Orbitale – prl, Prominentia laterale – pr, Prosthion – prd, Prosthion dentale – rhi, Rhinion – st, Stephanion – zy, Zygion – zm, Zygomaxillare

Figure 5 - Skull front view



b, Bregma – co, Coronale – eu, Eurion – ft, Frontotemporale – g, Glabella – l, Lambda – op, Opisthokranion – rhi, Rhinion – st, Stephanion – zy, Zygion

Figure 7 - Skull top view



Ba, Basion – b, Bregma – enm, Endomalare – g, Glabella – gn, Gnathion – ho, Hormion – i, Inion – id, Infracoronale – l, Lambda – li, Lingulare – n, Nasion – ns, Nasospinale – o, Opisthion – ol, Orale – op, Opisthokranion – pg, Pogonion – pr, Prosthion – rhi, Rhinion – spha, Sphenobasion – ss, Subspinale.

Figure 5 - Skull inside side view

Appendix B – Measures

These were the 24 measures used by the iDryas team to classify the skulls. The figures shown were taken from the master thesis of Catarina Coelho (Coelho, 2012), one of the team's specialists.

1. ZYB (bizygomatic width): the distance between both *Zygion* points;
2. BBH (*Basion-Bregma* height): distance between *Basion* and *Bregma*;
3. XCB (maximum skull width): maximum width perpendicular to the sagittal plane;
4. GOL (maximum skull length): distance (straight line) between *Glabella* and *Opisthokranion*;
5. BNL (*Nasion-Basion* length): distance between *Basion* and *Nasion*;
6. FRC (frontal line): distance, in the sagittal plane, between the *Nasion* and *Bregma*;



7. BPL (*Basion-Prosthion* length): the distance (strait line) between *Basion* and *Prosthion*;



8. UFHT (superior facial height): distance between *Nasion* and *Prosthion*;



9. MAB (*maxillo-alveolar* width): is the maximum width of the alveolar arch on the outer surface (the distance between both *Ektomalare* points);



10. AUB (*Biauricular* width): the minimum exterior width measured in the root of the zygomatic processes;



11. NLH (*nasal height*): distance between the *Nasion* and *Naso-spinale*;



12. UFBR (*superior facial width*): distance between both *Frontomolare-Temporale* points;



13. PAC (*parietal line*): distance, in the sagittal plane, between *Bregma* and *Lambda*;



14. FOL (length of the *Foramen Magnum*): distance between *Basion* and *Opisthion*;



15. WFB (minimum facial width): distance between both *Fronto-temporale* points;



16. NLB (nasal width): maximum width of the nasal aperture;



17. OBB (orbital width): distance between *Dakyon* and *Ektokonchion*;



18. OBH (orbital height): distance between the border of the inferior and superior orbit.



19. EKB (bi-orbital width): distance between both *Ektokonchion* points;



20. DKB (inter-orbital width): distance between both *Dakyon* points;



21. OCC (occipital line): distance, in the sagittal plane, between *Lambda* and *Opisthion*;



22. FOB (width of the *Foramen Magnum*): distance between the lateral margins of the *Foramen Magnum*, in the lateral point with biggest curvature;



23. MAL (*maxillo-alveolar* length): distance between the *Prosthion* and *Alveolon*;



24. MDH (height of the *Mastoid process*): distance, in projection, between the *Frankfurt plane* and the nadir point of the *Mastoid process*;



Appendix C – Tables of Measures for all (8)

Skulls

The tables in this appendix show the measures taken by the domain experts using CraMs (App) and traditional methods (Antr). Measures with the value β (highlighted in bold) were considered to be difficult to obtain by the experts for that specific specimen.

Measure	Specimen #21				Specimen #25			
	User #1		User #2		User #1		User #2	
	App	Antr	App	Antr	App	Antr	App	Antr
1 - ZYB	β	β	β	β	136,7	136	136,7	137
2 - BBH	β	β	β	β	142,7	142	142,7	143
3 - XCB	127,5	124	127,5	126	135	131	135	131
4 - GOL	171,6	172	171,3	169	182,1	181	182,1	181
5 - BNL	β	β	β	β	105,3	106	105,3	107
6 - FRC	107,6	108	107,6	108	116,6	114	116,6	115
7 - BPL	β	β	β	β	102,8	103	102,8	104
8 - UFHT	60,1	62	64,1	65	64,6	62	64,8	64
9 - MAB	56,6	57	57,6	59	65,3	66	65,7	65
10 - AUB	100,9	98	101,4	98	116,9	110	114,6	108
11 - NLH	49	46	49	46	48,5	47	48,5	46
12 - UFBR	94,1	95	94	95	106,7	106	106,7	109
13 - PAC	108,2	103	108,4	104	115,3	115	114,7	116
14 - FOL	β	β	β	β	40	39	40,8	38
15 - MAL	β	β	β	β	54,3	56	53	58
16 - MDH	25,4	24	22	22	31,5	31	28,8	32
17 - OBB	39,8	40	39,6	38	44,1	47	42,6	43
18 - OBH	31,8	34	32,2	31	35,3	35	34,9	33
19 - WFB	84,3	86	84,3	86	99,7	101	98,5	101
20 - NLB	26,4	28	29,8	27	27,6	28	28,8	27
21 - EKB	91,3	89	87,9	87	102,4	100	98,9	100
22 - DKB	β	β	β	β	β	β	β	β
23 - OCC	88,4	87	87,9	89	93,6	94	93,5	96
24 - FOB	30,2	33	32,3	32	28,9	29	31,7	29

Measure	Specimen #38				Specimen #39			
	User #1		User #2		User #1		User #2	
	App	Antr	App	Antr	App	Antr	App	Antr
1 - ZYB	119,4	119	117,4	121	β	β	β	β
2 - BBH	132,9	133	132,9	133	133	132	133	133
3 - XCB	137,7	136	137,7	137	121,3	114	121,3	117
4 - GOL	180,1	180	179,7	175	167,7	169	167,3	164
5 - BNL	95,2	95	95,2	96	88,9	84	88,9	90
6 - FRC	109,1	112	109,1	107	106,7	98	106,7	98
7 - BPL	β	β	β	β	92,3	93	93,6	92
8 - UFHT	β	β	β	β	56	54	58,7	56
9 - MAB	62	61	61,6	61	β	β	β	β
10 - AUB	105,5	101	102,9	101	102	100	101,7	98
11 - NLH	50	48	50	47	44,2	44	44,2	44
12 - UFBR	98,2	98	96,6	99	90	92	89,8	94
13 - PAC	116,2	114	117	119	109	114	108,5	114
14 - FOL	34,1	32	35,4	31	33	33	35,1	31
15 - MAL	β	β	β	β	51,7	50	50,7	50
16 - MDH	27,7	26	27,6	27	22,6	20	22,1	22
17 - OBB	43,1	45	42,4	42	40,4	43	40,7	40
18 - OBH	39,5	39	36,6	36	30,9	32	29,4	29
19 - WFB	89,1	91	88,4	90	77	79	75,9	79
20 - NLB	23,6	24	26,5	24	26,1	27	27,9	25
21 - EKB	92,5	95	93,9	93	90	89	91,5	87
22 - DKB	19,6	21	17,6	20	15,6	16	14,9	16
23 - OCC	96,3	97	94,8	98	93	93	91,6	94
24 - FOB	23,6	25	25,9	22	27	28	28,2	26

Measure	Specimen #57				Specimen #65			
	User #1		User #2		User #1		User #2	
	App	Antr	App	Antr	App	Antr	App	Antr
1 - ZYB	β	β	β	β	136,2	134	136,2	136
2 - BBH	β	β	β	β	138,8	139	140,1	139
3 - XCB	138,6	137	138,6	137	β	123	β	124
4 - GOL	184,9	185	184,3	182	174,8	175	174,8	175
5 - BNL	β	β	β	β	105,5	106	105	106
6 - FRC	120,3	116	120,3	115	110,7	109	114,6	109
7 - BPL	β	β	β	β	103,9	103	104,8	105
8 - UFHT	56,2	57	59,9	58	56,5	56	60	60
9 - MAB	60,9	61	61,2	61	63,5	62	63,8	64
10 - AUB	112,9	108	108,3	109	109,8	102	106,7	99
11 - NLH	43,2	44	43,2	44	45,9	45	43	44
12 - UFBR	99,6	101	99,4	103	109,2	113	111,8	114
13 - PAC	114,2	120	115,1	119	116,2	116	113,8	116
14 - FOL	β	β	β	β	38	36	39,1	36
15 - MAL	51,9	55	50,9	54	57,3	57	56,3	57
16 - MDH	25,4	23	27	22	29,6	31	29,5	32
17 - OBB	42,7	43	43	43	43,2	43	42,9	42
18 - OBH	32,8	33	32,7	32	33,8	34	33,2	33
19 - WFB	93,8	97	91,7	95	105	107	103,7	107
20 - NLB	25,1	27	26,7	24	32	34	32,4	30
21 - EKB	96,5	97	96,1	91	106,3	100	105,2	97
22 - DKB	24,3	β	21	β	28,5	β	24,9	β
23 - OCC	β	β	β	β	92,1	91	91	91
24 - FOB	β	β	β	β	29	28	29,5	28

Measure	Specimen #66				Specimen #67			
	User #1		User #2		User #1		User #2	
	App	Antr	App	Antr	App	Antr	App	Antr
1 - ZYB	β	β	β	β	126,5	126	126,5	126
2 - BBH	129,8	130	130,3	130	131	131	131	130
3 - XCB	β	133	β	137	131,5	122	131,5	126
4 - GOL	185,3	186	185,3	179	182	182	182	173
5 - BNL	95,9	96	96,9	97	104,6	104	104,6	105
6 - FRC	120	113	120	112	109,6	107	109,6	108
7 - BPL	97,8	94	100,3	99	100	94	100,7	102
8 - UFHT	55,1	57	57,8	58	63,4	64	65,6	66
9 - MAB	60,9	60	60	61	60,1	61	59,1	61
10 - AUB	122,8	123	120,4	114	110,4	107	107,7	107
11 - NLH	42,7	44	42,7	43	49,6	49	49,2	49
12 - UFBR	105,4	107	103,8	108	105,2	106	105,3	108
13 - PAC	103,1	109	101,4	108	105,5	106	105,9	105
14 - FOL	39,2	37	38,3	37	33,3	32	33,6	32
15 - MAL	57,1	56	57,6	60	54	57	53,6	59
16 - MDH	30,6	28	32,9	33	25,8	27	23,5	25
17 - OBB	43,9	42	44,1	43	46,5	43	46,6	42
18 - OBH	31,2	32	33	30	33,8	34	34,2	32
19 - WFB	94,7	97	93,8	96	93,6	96	92,7	95
20 - NLB	29	30	29,8	27	26,4	26	27,2	25
21 - EKB	98,9	95	99,5	96	100,8	99	100,5	98
22 - DKB	26,2	27	25,5	29	27	27	21	26
23 - OCC	108,4	111	108,7	111	96,7	97	96,3	97
24 - FOB	35,1	32	36,5	31	31,6	30	33,4	30

Appendix D – Tables of Measures for all (8)

Skulls using Decimated models

These tables show the automatic measures obtained for all eight specimens using different reduction percentages. Not all three automatic measures were available for all specimens due to fractures or incorrect automatically detected points. Measures highlighted in bold were considered to have an unacceptable error.

	Specimen #21						
	100%	80%	60%	40%	20%	10%	5%
XCB	127,48	127,49	127,46	127,25	127,35	127,48	127,01

	Specimen #25								
	100%	80%	60%	40%	20%	10%	5%	2.5%	1%
ZYB	136,70	136,73	136,73	136,73	136,74	136,75	136,74	136,71	137,25
BBH	142,70	142,70	142,70	142,70	142,70	142,72	142,71	142,71	57,19
XCB	135,00	135,03	135,03	135,03	135,04	136,66	135,04	136,44	135,61

	Specimen #38						
	100%	80%	60%	40%	20%	10%	5%
BBH	132,90	132,99	133,25	133,28	132,99	133,18	133,02
XCB	137,70	137,70	137,72	137,70	137,56	137,66	137,69

	Specimen #39						
	100%	80%	60%	40%	20%	10%	5%
ZYB	117,30	117,27	117,28	117,29	117,29	117,30	117,30
BBH	132,90	133,18	133,01	133,96	133,43	132,97	133,19
XCB	121,30	121,37	121,79	121,17	121,20	121,21	121,22

	Specimen #57						
	100%	80%	60%	40%	20%	10%	5%
XCB	138,61	138,62	138,59	138,59	138,61	138,64	138,63

	Specimen #65								
	100%	80%	60%	40%	20%	10%	5%	2.5%	1%
ZYB	136,2	136,2	136,2	136,2	136,2	136,2	136,2	136,3	136,4
BBH	140,2	140,2	140,2	140,2	140,2	140,1	140,0	138,5	102,6
XCB	130,3	130,3	130,3	130,3	130,3	130,2	130,2	130,1	146,2

	Specimen #66						
	100%	80%	60%	40%	20%	10%	5%
BBH	130,31	130,35	130,28	130,22	130,21	130,31	130,24
XCB	142,08	142,08	143,32	141,96	142,08	143,26	142,10

	Specimen #67						
	100%	80%	60%	40%	20%	10%	5%
ZYB	126,50	126,52	126,53	126,54	126,54	126,51	126,55
BBH	131,00	131,02	131,04	130,93	131,05	131,02	130,98
XCB	131,50	129,08	128,92	129,67	128,93	127,80	129,84

Appendix E – Tables of Measures for all (8)

Skulls using the orbit detection method

These tables show the results obtained for all eight specimens by the author with the orbit detection method (App) and by the two domain experts using traditional methods (Antr). Measurements with the value β (highlighted in bold) were considered to be difficult to obtain by the experts for that specific specimen.

	Specimen #21			Specimen #25			Specimen #38		
	App	Antr #1	Antr #2	App	Antr #1	Antr #2	App	Antr #1	Antr #2
OBB	40,2	40	38	43,6	47	43	42,3	45	42
OBH	32,8	34	31	34,2	35	33	36,6	39	36
EKB	94,1	89	87	105	100	100	95,2	95	93
DKB	21,9	β	β	27,6	β	β	18,6	21	20

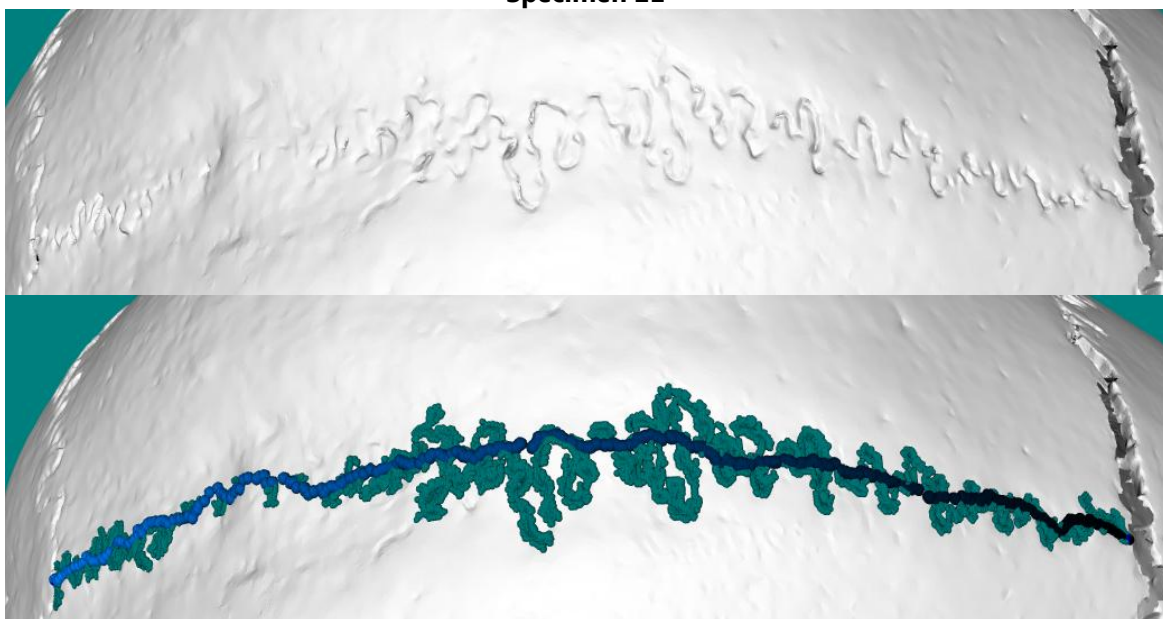
	Specimen #39			Specimen #57			Specimen #65		
	App	Antr #1	Antr #2	App	Antr #1	Antr #2	App	Antr #1	Antr #2
OBB	38,7	43	40	41,9	43	43	42,4	43	42
OBH	29,6	32	29	32,4	33	32	32,8	34	33
EKB	92,1	89	87	101	97	91	107	100	97
DKB	14,5	16	16	21,7	β	β	27,5	β	β

	Specimen #66			Specimen #67		
	App	Antr #1	Antr #2	App	Antr #1	Antr #2
OBB	41,5	42	43	43,4	43	42
OBH	31,6	32	30	33,5	34	32
EKB	101	95	96	104	99	98
DKB	23,9	27	29	23,1	27	26

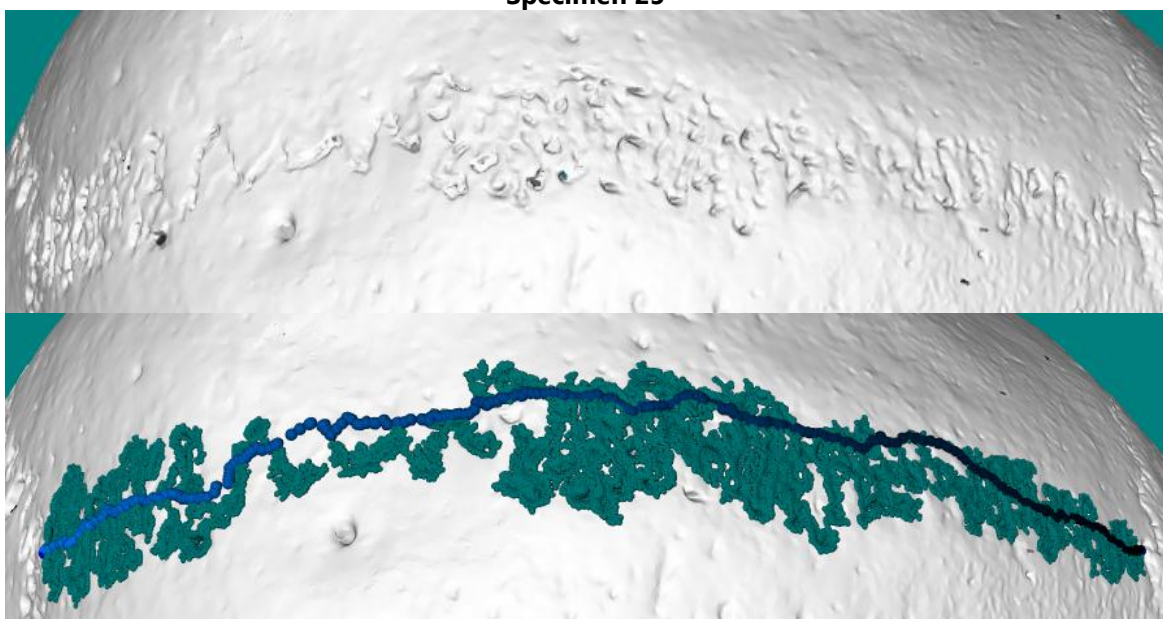
Appendix F – Figures of the Sagittal suture detected in all (8) Skulls

This appendix shows the figures of the Sagittal sutures before (top) and after (bottom) they are detected using the Sharp Edge method (explained in section 4.4.2.) in all eight skulls.

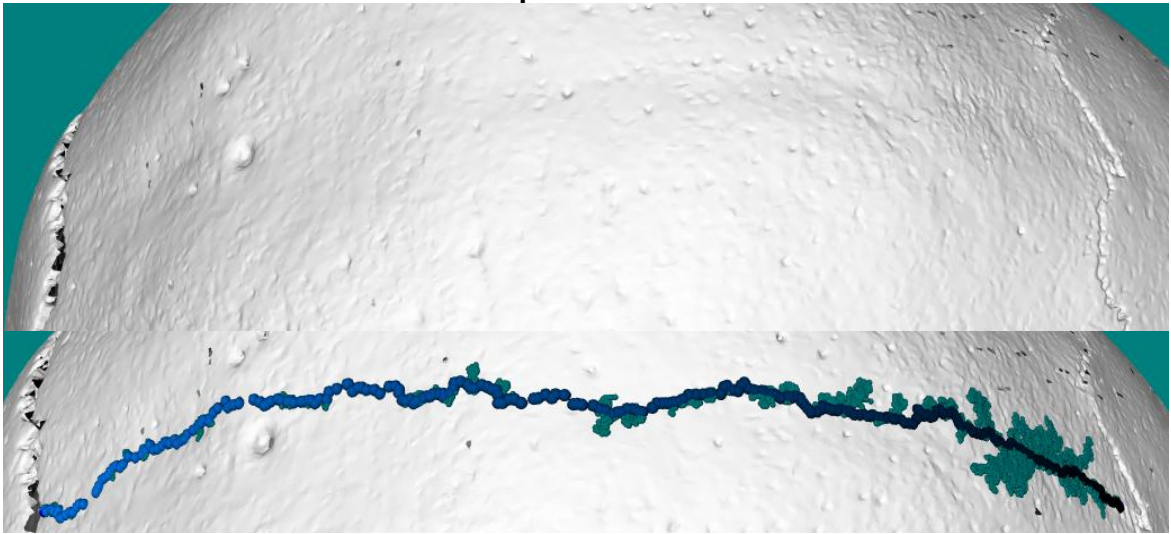
Specimen 21



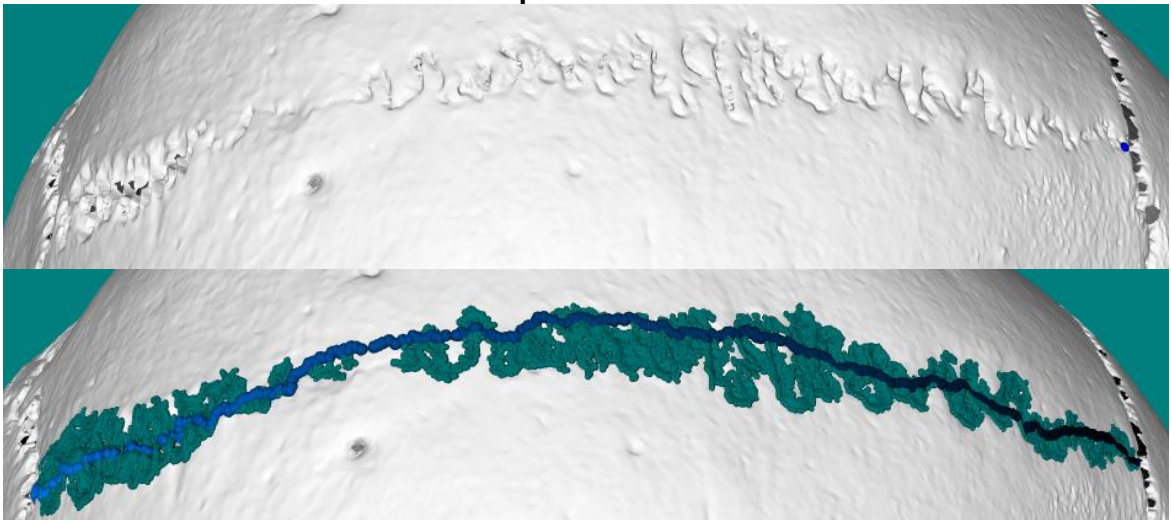
Specimen 25



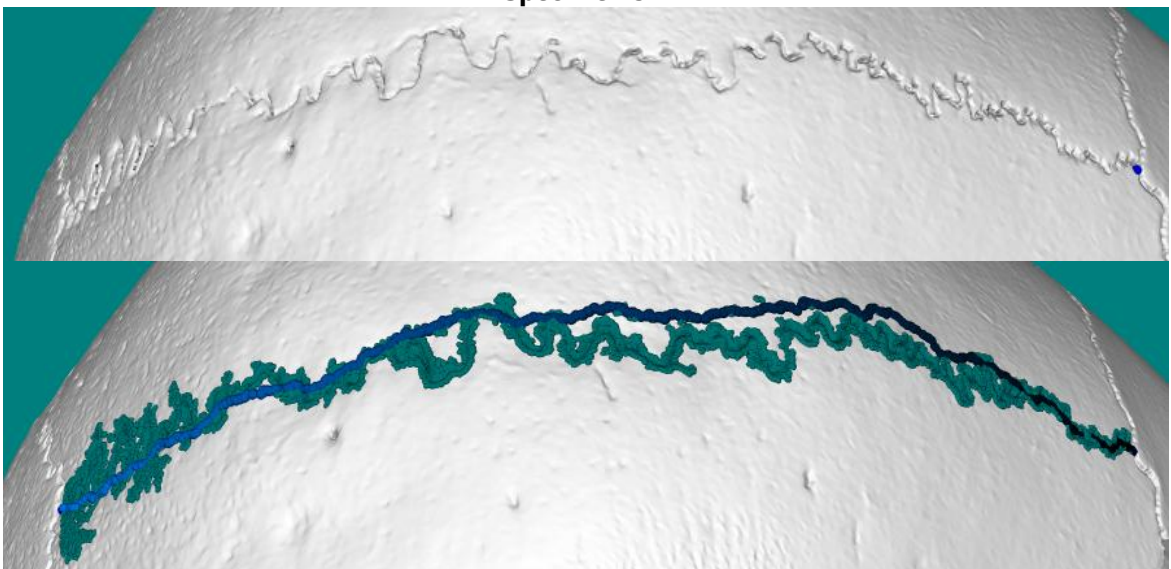
Specimen 38



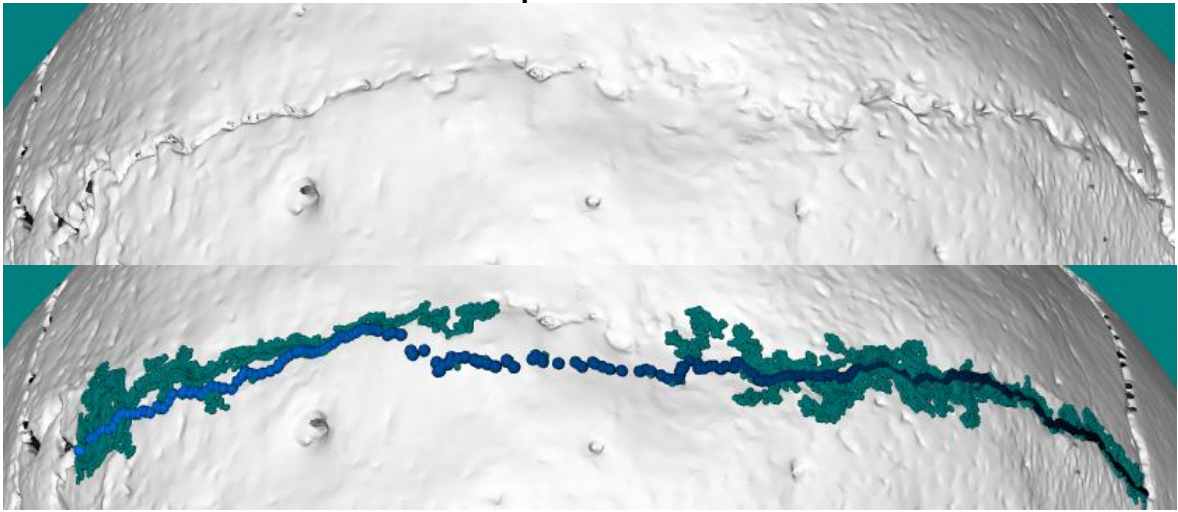
Specimen 39



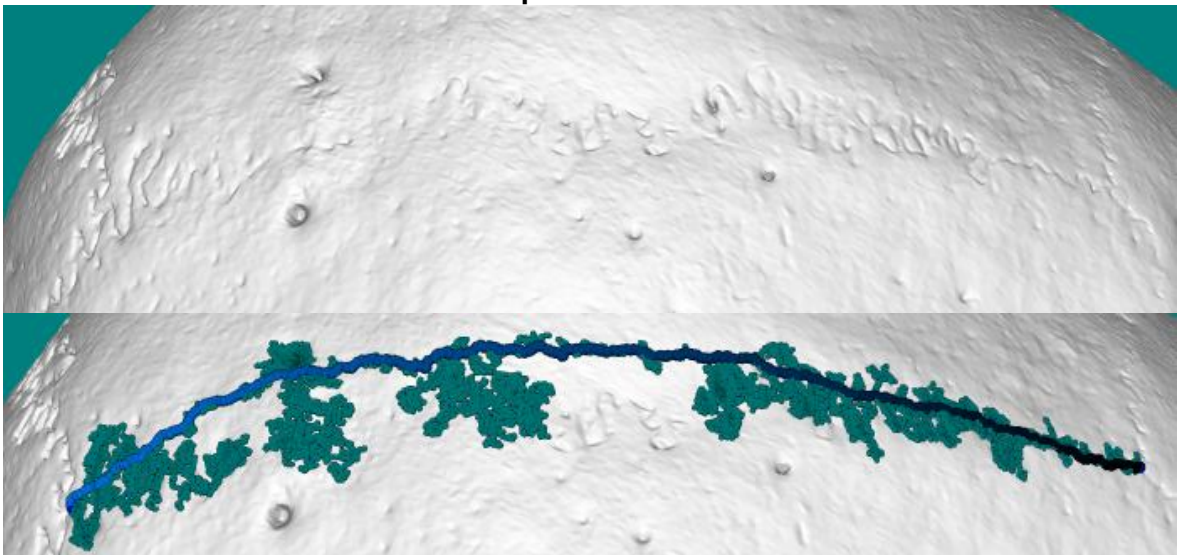
Specimen 57



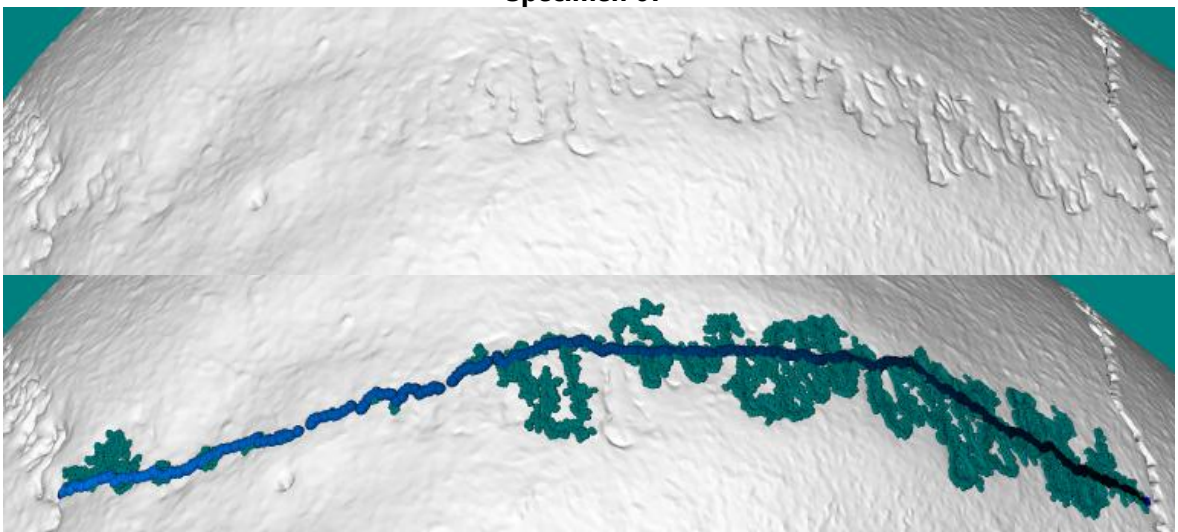
Specimen 65



Specimen 66



Specimen 67



Appendix F – CraMs User Manual

This appendix serves as a manual to the usage of the CraMs application.

File Menu

In this menu it is possible to open a model with the extension ".ply" as shown in Figure 1.

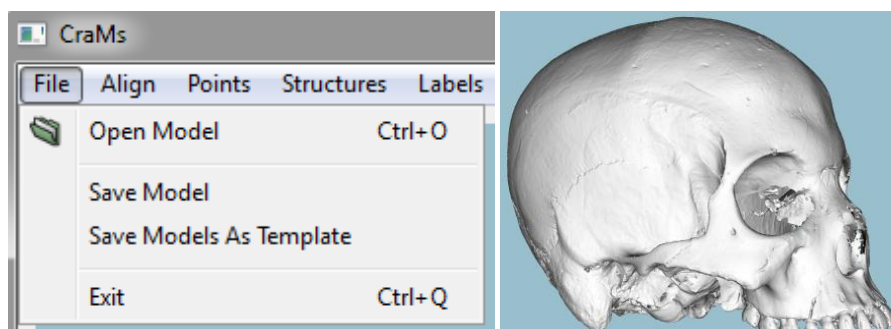


Figure 1 - Open Model menu (left) and the result (right)

It is also possible to save the model (normally or as a template) and exit the application.

Align Menu

It is possible to align the model manually by picking seven reference points. During the manual alignment it is possible to restart the process. Press the Align button when all points are marked.

Figure 2 shows the Manual align menu.

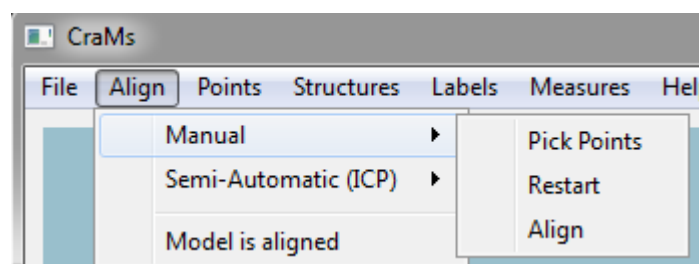


Figure 2 - Manual align menu

It is recommended the usage of the Semi-Automatic alignment method. Before loading the template the user can check or uncheck the option to align centroids as explained at the end of section 3.2.2. Then load the template model (".ply" file). Figure 3 shows the Semi-Automatic align menu

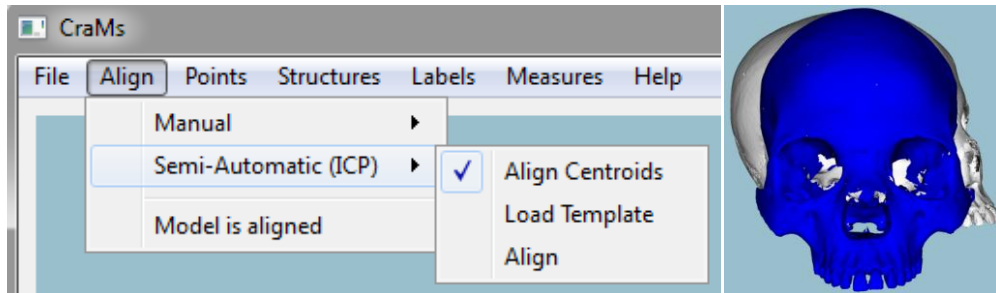


Figure 3 - Semi-Automatic menu (left) and the result of loading a Template model (right)

After loading a template it is possible to pre-align the two models manually with the x, y and z key (using the shift key to change the direction). When the orientation of the models is similar click the Align button to start the process. Figure 4 illustrates the process.

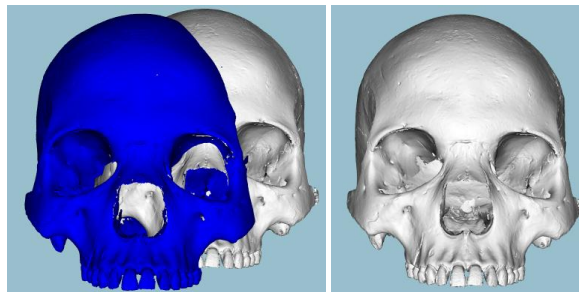


Figure 4 - Optimal orientation (left) and the result of the alignment (right)

If the model is already aligned it is possible to skip the alignment process by clicking the "Model is aligned" button in the Align menu.

Points Menu

After the skull is aligned it is possible to mark points. Some of them can be marked automatically by using the *Try Automatic* button. These points can be deleted and marked manually through the *Correct Automatic Points* sub-menu as shown in Figure 5.

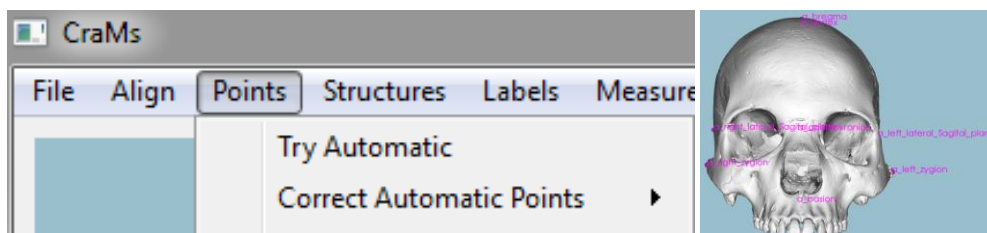


Figure 5 - Automatic points sub-menu (left) and the result of the "Try Automatic" button (right)

From this menu it is also possible to mark the rest of the points. Some keys may be useful for this process (see Additional keys section for more information). Some of the points are defined using neighbourhood while others are fully manual, as shown in Figure 6. All points can be deleted.

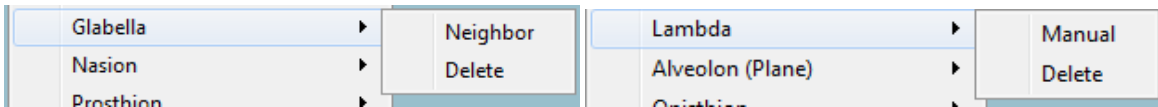


Figure 6 - Example of points defined using neighbourhood (left) and fully manual (right)

A fully marked skull should look something like what is shown in Figure 7.

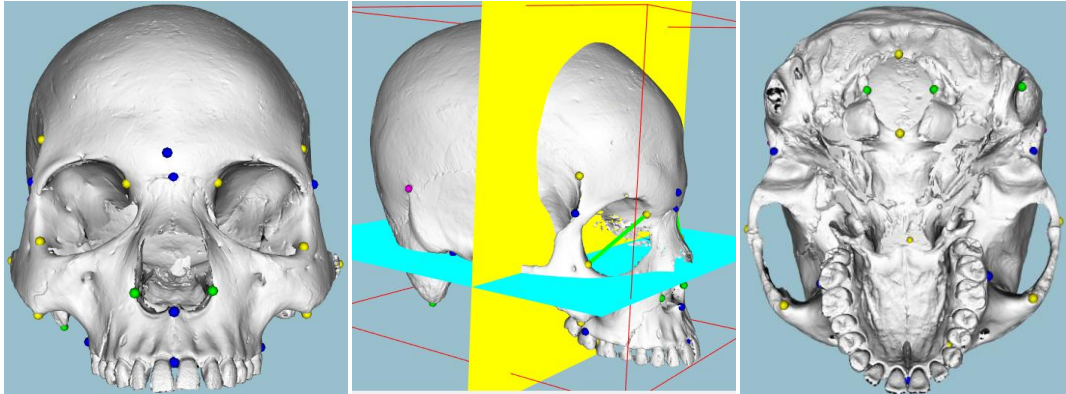


Figure 7 - Fully marked skull front (left), side with planes (middle) and bottom (right) view

From this menu it is also possible to delete all marked points.

Structures Menu

From here it is possible to detect structures such as the orbits and sutures. For the orbits it is possible to mark two structures (right and left) as shown in Figure 8. Use the Sharp Edges method and follow the instructions given to detect the orbits. You can also delete or hide the detected structures.

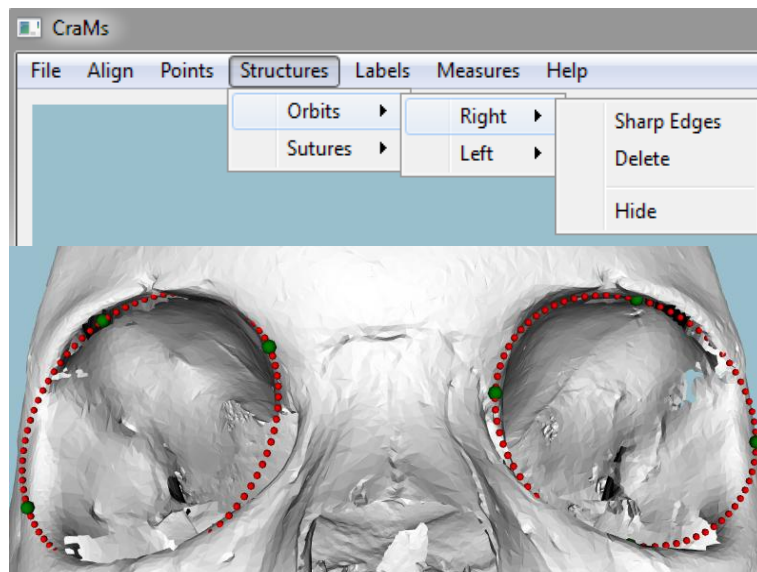


Figure 8 - Orbits structure sub-menus (top) and results of having both orbits detected (bottom)

The suture detection method is similar to the orbit detection method but uses only two reference points. The two points should be marked at the extremities of the suture. Figure 9 shows the results obtained from using this method.

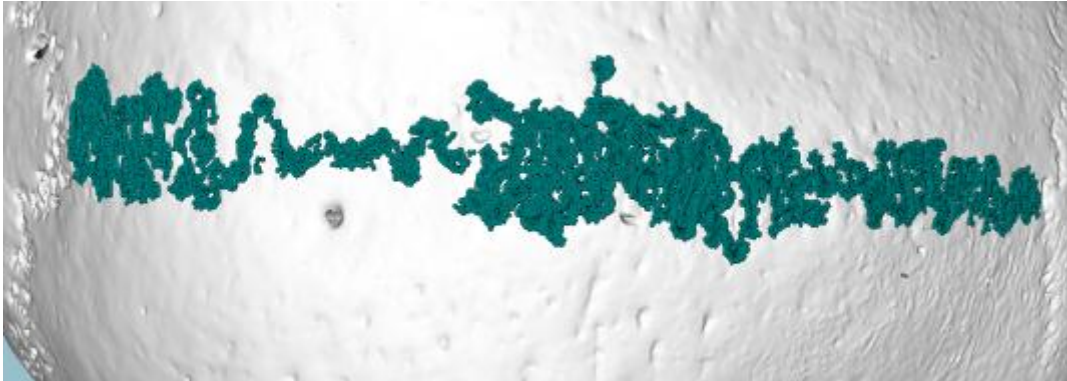


Figure 9 - Results of the suture detection method

Labels Menu

From this menu it is possible to show or hide the labels for each category of points marked. Figure 10 shows the Labels menu. These can be used to identify which are the marked points.



Figure 10 - Labels menu

Measures Menu

When all the desired points are marked it is possible to calculate the measures through the *Measures* menu. From this menu it is also possible to read the points marked from a saved file and to see the list of measures. If any point is missing a warning will be presented. Figure 11 shows the Measures menu and an example of the warning.

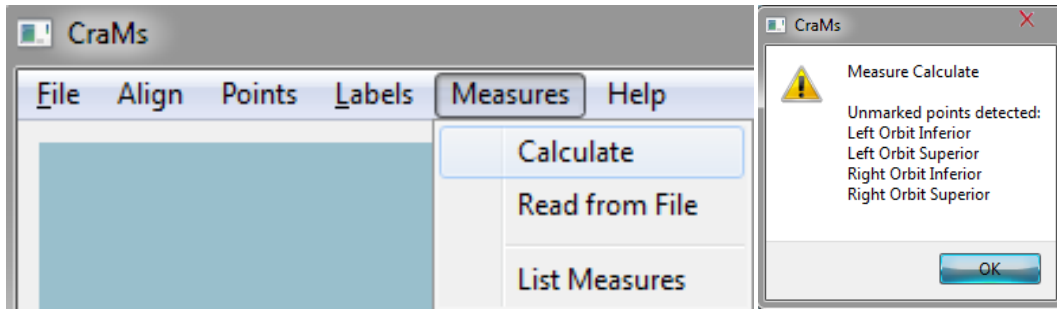


Figure 11 - Measures menu (left) and unmarked points warning (right)

When the warning is presented the user must choose to go back and mark the missing points or to ignore them and proceed with the calculation, as shown in Figure 12.

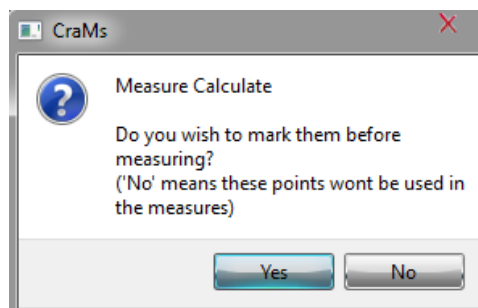


Figure 12 - Confirmation menu

After the calculations all the measures are presented and the user can go back (by clicking the OK button) or save them, as shown in Figure 13.

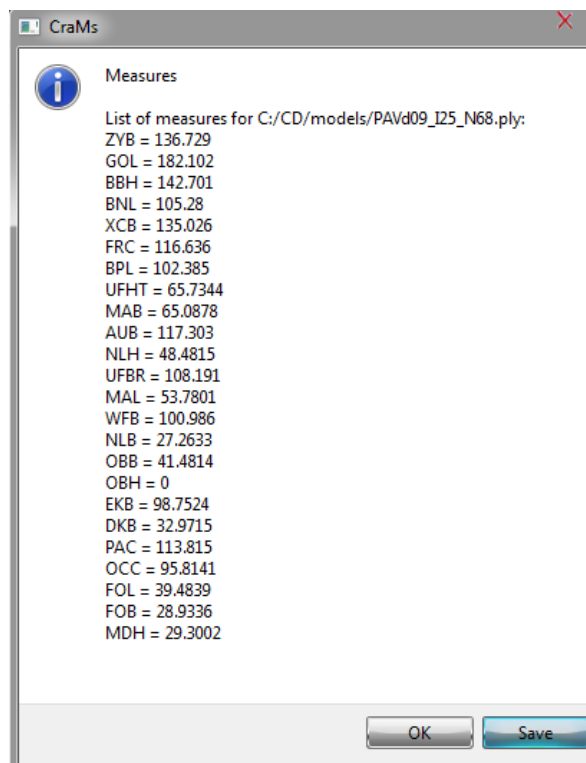


Figure 13 - List of measures

Finally the user can type his name (shown in Figure 14) and choose the destination of the measures file.

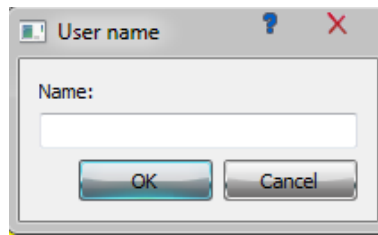


Figure 14 - Name input menu

Additional keys

There are a couple of useful keys that might help and improve the usage of the application.

These two can be used to mark points more accurately:

- The "F" key can be used to focus on the point the mouse pointer is;
- The "R" key resets the view (removing focus).

These keys can be used to manipulate the model and the view:

- "Control" key can be used to rotate the model;
- "Shift" key can be used to drag the model;
- Holding the left mouse button and moving the cursor will rotate the model;
- Scrolling up or down on the middle mouse button will zoom in or out.

By right clicking on the display area it is possible to access a menu that has a couple of functionalities. These include changing the background colour and toggling the visibility of many different objects. This menu is shown in Figure 15.

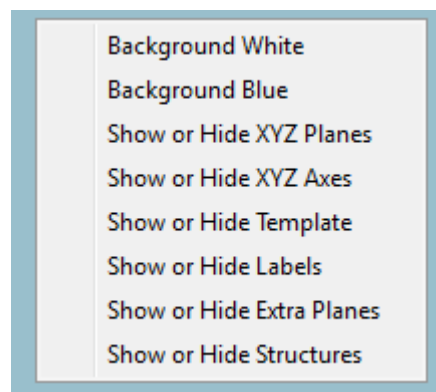


Figure 15 - Right click menu

Appendix G – CraMs Installation and Configuration

This appendix serves as a manual to the installation and configuration of the CraMs project using Visual Studio 2010.

Libraries used(make sure to include them in the Path Environment Variable):

- VTK 5.10.1
- QT 4.8.5
- Wild Magic 5.11
- Boost 1.55.0

C/C++ -> General -> Additional Include Directories:

- boost\boost_1_55_0;
- GeometricTools\WildMagic5\SDK\Include;
- VTK/include/vtk 5.10;
- Qt/4.8.5/include;
- Qt/4.8.5/include/QtGui;
- Qt/4.8.5/include/QtCore;
- «Code folder».

C/C++ -> Preprocessor -> Preprocessor Definitions:

- QT_DLL;
- QT_GUI_LIB;
- QT_CORE_LIB;
- QT_NO_DEBUG;
- WM5_CORE_DLL_IMPORT;
- WM5_MATHEMATICS_DLL_IMPORT;
- WM5_CORE_IMPORT_DLL;
- WM5_MATHEMATICS_IMPORT_DLL;
- CMAKE_INTDIR="Release".

Linker -> Input -> Additional Dependencies:

- VTK lib files:
QVTK.lib; vtkRendering.lib; vtkGraphics.lib; vtkIO.lib; vtkCommon.lib; vtkViews.lib; vtkIn-fovis.lib; vtkWidgets.lib; vtkHybrid.lib; vtkexoIIC.lib; vtkVolumeRendering.lib; vtkverdict.lib; vtkImaging.lib; vtk-5.10\vtkftgl.lib; vtk-5.10\vtkfreetype.lib; vtkFiltering.lib; vtkDICOM-Parser.lib; vtkNetCDF_cxx.lib; vtkNetCDF.lib; vtkhdf5_hl.lib; vtkhdf5.lib; LSDyna.lib; vtkmetaio.lib; vtksqlite.lib; vtkpng.lib; vtktiff.lib; vtkjpeg.lib; vtkexpat.lib; vtksys.lib; vtklibxml2.lib; vtkzlib.lib; vtkalglib.lib.
- QT lib files:
QtGui4.lib; QtCore4.lib; QtWebKit4.lib; QtXmlPatterns4.lib; QtNetwork4.lib; QtSql4.lib.
- Wm5 lib files:
Wm5Core.lib; Wm5Mathematics.lib